

3 mm spectral line survey of two lines of sight toward two typical cloud complexes in the Galactic Center

J. Armijos-Abendaño^{1*}, J. Martín-Pintado¹, M. A. Requena-Torres², S. Martín³
and A. Rodríguez-Franco⁴

¹*Centro de Astrobiología (INTA-CSIC), Ctra a Ajalvir, km 4, 28850, Torrejón de Ardoz, Madrid, Spain*

²*Max-Planck Institut für Radioastronomie, Auf dem Hügel 69, D-53121 Bonn, Germany*

³*European Southern Observatory, Alonso de Córdova 3107, Vitacura, casilla 19001, Santiago 19, Chile*

⁴*Facultad de Óptica y Optometría, Departamento de Matemática Aplicada (Biomatemática), Universidad Complutense de Madrid, Avenida de los Arcos de Jalón, 118, E-28037 Madrid, Spain*

Accepted 2013 March 15. Received 2013 March 30; in original form 1988 October 11

ABSTRACT

We present the results of two Mopra 3-mm spectral line surveys of the Lines of Sight (*LOS*) toward the Galactic Center (GC) molecular complexes Sgr B2 (*LOS*+0.693) and Sgr A (*LOS*−0.11). The spectra covered the frequency ranges of ~77–93 GHz and ~105–113 GHz. We have detected 38 molecular species and 25 isotopologues. The isotopic ratios derived from column density ratios are consistent with the canonical values, indicating that chemical isotopic fractionation and/or selective photodissociation can be considered negligible (<10%) for the GC physical conditions. The derived abundance and rotational temperatures are very similar for both *LOS*s, indicating very similar chemical and excitation conditions for the molecular gas in the GC. The excitation conditions are also very similar to those found for the nucleus of the starburst galaxy NGC 253. We report for the first time the detection of HCO and HOC⁺ emission in *LOS*+0.693. Our comparison of the abundance ratios between CS, HCO, HOC⁺ and HCO⁺ found in the two *LOS*s with those in typical Galactic photodissociation regions (PDRs) and starbursts galaxies does not show any clear trend to distinguish between UV and X-ray induced chemistries. We propose that the CS/HOC⁺ ratio could be used as a tracer of the PDR components in the molecular clouds in the nuclei of galaxies.

Key words: Galaxy: centre – ISM: clouds – ISM: molecules.

1 INTRODUCTION

In this paper we study the physical conditions and chemical complexity of the quiescent molecular gas along two Lines of Sight (*LOS*), one toward the Sgr B2 complex (*LOS*+0.693) and the other one toward the Sgr A complex (*LOS*−0.11), both complexes located in the Galactic Center (GC). Molecular cloud complexes inside the Central Molecular Zone (CMZ, Morris & Serabyn (1996)) in the GC show very different characteristics that the clouds in the Galactic disc. GC clouds are characterized by high gas-kinetic temperatures of $\gtrsim 100$ K (Hüttemeister et al. 1993; Rodríguez-Fernández et al. 2001) and cold dust temperatures (T_{dust}) of $\lesssim 30$ K (Rodríguez-Fernández et al. 2004).

The Sgr B2 complex contains one of the most outstanding massive star formation sites in the Galaxy and consists

of several star-forming cores embedded in a lower density envelope (Gordon et al. 1993). Sgr B2 hosts many dozens of compact and hypercompact HII regions, e.g., De Pree et al. (1996, 1998) concentrated in two regions, Sgr B2N and Sgr B2M. *LOS*+0.693 toward the Sgr B2 molecular complex studied in this paper, shown in Fig. 1 (upper and middle panels), is outside the HII region L (Mehringer et al. 1995) and the main massive star forming regions Sgr B2M and Sgr B2N (Martín-Pintado et al. 1990). Therefore, *LOS*+0.693 does not appear to be affected strongly by UV radiation, but otherwise this *LOS* may be subjected to significant X-ray irradiation since the Sgr B2 cloud is a well established X-ray reflection nebula due to its strong Fe K α line emission at 6.4 keV (Koyama et al. 1996).

The Sgr A molecular complex contains two massive molecular clouds at 20 km s^{−1} and 50 km s^{−1} believed to be interacting with the Circumnuclear Disk (CND) surrounding the central supermassive black hole Sgr A* and two super-

* E-mail: armijosaj@cab.inta-csic.es

nova remnants, Sgr A East and G359–0.09 (Coil & Ho 2000; Herrnstein & Ho 2002; Ferrière 2012). LOS –0.11 toward the 20 km s^{–1} molecular cloud, shown in Fig. 1 (bottom panels), is located in projection 216'' (~8.6 pc) south of the black hole Sgr A*. LOS –0.11, lies near the elongated non-thermal features Sgr A-F and Sgr A-E (Yusef-Zadeh & Morris 1987; Lu et al. 2003; Yusef-Zadeh et al. 2005) indicated in Fig. 1. Recent star formation (compact HII regions G–0.02–0.007) around Sgr A* is mainly concentrated toward the 50 km s^{–1} molecular cloud (Mills et al. 2011).

Unlike the star forming regions of Sgr B2M and Sgr B2N, the selected lines of sight toward the cloud positions in the Sgr B2 and Sgr A complexes studied in this paper do not show any signposts of massive star formation like H₂O masers, ultracompact HII regions, hot cores or recombination line emission (Hüttemeister et al. 1993; Martín-Pintado et al. 1997).

Several unbiased spectral line surveys have been carried out toward the Sgr B2 star forming cores, positions N (Nummelin et al. 1998, 2000; Friedel et al. 2004; Belloche et al. 2013), M (Sutton et al. 1991; Belloche et al. 2013), S and OH (Friedel et al. 2004). Nummelin et al. (1998, 2000) also carried out a spectral survey toward a quiescent region in Sgr B2. They detected 26 species and showed the large difference in chemical complexity and excitation between the quiescent and the star forming clouds. Our line survey of two quiescent lines of sight were selected from the systematic study of the HNC/CS ratios carried out by Martín et al. (2008). In this study both locations were among the objects which showed the highest ratios indicating that the chemistry and likely the heating of both GC LOS s are mainly dominated by low velocity shocks. This is also supported by Requena-Torres et al. (2008), who also studied several GC sources, including our two LOS s, finding that the abundances of complex organic molecules like CH₂OHCHO, (CH₃)₂O, CH₃CHO, among others, are larger in these GC LOS s than those in hot cores of the Galactic disk, suggesting ejection of molecules from dust grains by low velocity C-type shocks. Previous surveys of the Sgr B2 quiescent clouds by Nummelin et al. (1998, 2000) at high frequencies did not have the sensitivity to detect weak molecular lines from these species.

In this paper, we present a 3 mm spectral line survey of the quiescent molecular gas along LOS +0.693 and LOS –0.11 toward the Sgr B2 and Sgr A complexes, respectively. Both complexes, inside the CMZ, are outstanding regions affected by high energy phenomena (Koyama et al. 1996; Terrier et al. 2010; Ponti et al. 2010) and large scale shocks (Martín-Pintado et al. 2001). Our sensitivity allowed us to detect, for the first time, the emission of the HCO and HOC⁺ molecules, which are considered to be tracers of UV radiation and X-ray chemistry in molecular clouds. In Sec. 2, we present our observations and data reduction. In Sec. 3, the details of the line identification (Sec. 3.1), line profiles (Sec. 3.2) and analysis (Sec. 3.3) are reported. In Sec. 3.4 we derive six isotopic ratios and discuss their implications. In Sec. 4, we discuss the molecular abundance and excitation conditions found in the GC and compare them with those in galactic nuclei (Sec. 4.1), and the implication of our detection of HCO and HOC⁺ in the UV and X-ray induced chemistry in galactic nuclei (Sec. 4.2). Finally, the conclusions are summarized in Sec. 5.

2 OBSERVATIONS AND DATA REDUCTION

The observations were carried out with the 22-m Mopra radio telescope¹ on November of 2007. We used the the dual 3 mm Monolithic Microwave Integrated Circuit (MMIC) receiver connected to the 8 GHz Spectrometer, which provided a velocity resolution of ~0.9 km s^{–1} at 90 GHz. Spectra in two polarizations were observed simultaneously. Two frequency ranges in the 3 mm window were covered, from ~77 to 93 GHz and from ~105 to 113 GHz. The beam size of the telescope was 38'' at 90 GHz and 30'' at 115 GHz. We used position switching as observing mode with the emission free reference positions selected from the CS maps obtained by Bally et al. (1987). The nominal positions used for the observation of LOS +0.693 and LOS –0.11 were $\alpha_{J2000} = 17^{\text{h}}47^{\text{m}}22^{\text{s}}.0$, $\delta_{J2000} = -28^{\circ}21'27''.0$ and $\alpha_{J2000} = 17^{\text{h}}45^{\text{m}}39^{\text{s}}.0$, $\delta_{J2000} = -29^{\circ}04'05''.0$, respectively. Fig. 1 shows the two observed positions superimposed on the SiO(2-1) (Martín-Pintado & Amo-Baladrón, priv. communication) and the 20 cm radio continuum maps (Yusef-Zadeh et al. 2004) of the Sgr B2 and Sgr A complexes. The reference positions were $\alpha_{J2000} = 17^{\text{h}}46^{\text{m}}23^{\text{s}}.0$, $\delta_{J2000} = -28^{\circ}16'37''.3$ and $\alpha_{J2000} = 17^{\text{h}}46^{\text{m}}00^{\text{s}}.1$, $\delta_{J2000} = -29^{\circ}16'47''.2$ for LOS +0.693 and LOS –0.11, respectively.

The raw data were reduced by using the ATNF Spectral Analysis Package (ASAP) at Mopra telescope to create the fits files for further processing with the MASSAJ package², where baseline subtraction were applied. In several regions of the spectra there were baseline ripples, which were partially corrected by editing the data in the Fourier transformed plane. The two polarizations of the spectra were averaged to improve the signal to noise ratio. The spectra were then smoothed to a velocity resolution of ~3.5 km s^{–1}, appropriate for the linewidths of ~20 km s^{–1} observed toward molecular clouds in the GC. Our line intensities in T_A^{*} units are affected by 20%-30% uncertainties in the calibration procedure based on a noise diode and an ambient temperature load.

3 RESULTS

3.1 Line identification

The 3 mm spectra observed toward both LOS s are shown in Fig. 2, where the identified molecules and the unidentified lines are indicated. A representative sample of line profiles for several molecular transitions and their isotopologues for LOS +0.693 and LOS –0.11 are shown in Fig. 3 and 4, respectively. The molecular identification and analysis were carried out using the frequencies and the spectroscopic information from the JPL (Pickett et al. 1998) and CDMS (Müller et al. 2001, 2005) catalogs contained in the MASSAJ package. For LOS +0.693, we found 38 molecular species and 25 isotopologues, as well as 18 unidentified

¹ Mopra is operated by the Australia Telescope National Facility, CSIRO and the University of New South Wales.

² This package have been developed at the Centro de Astrobiología. More information about this package in <http://damir.iem.csic.es/mediawiki-1.12.0/index.php/Portada>.

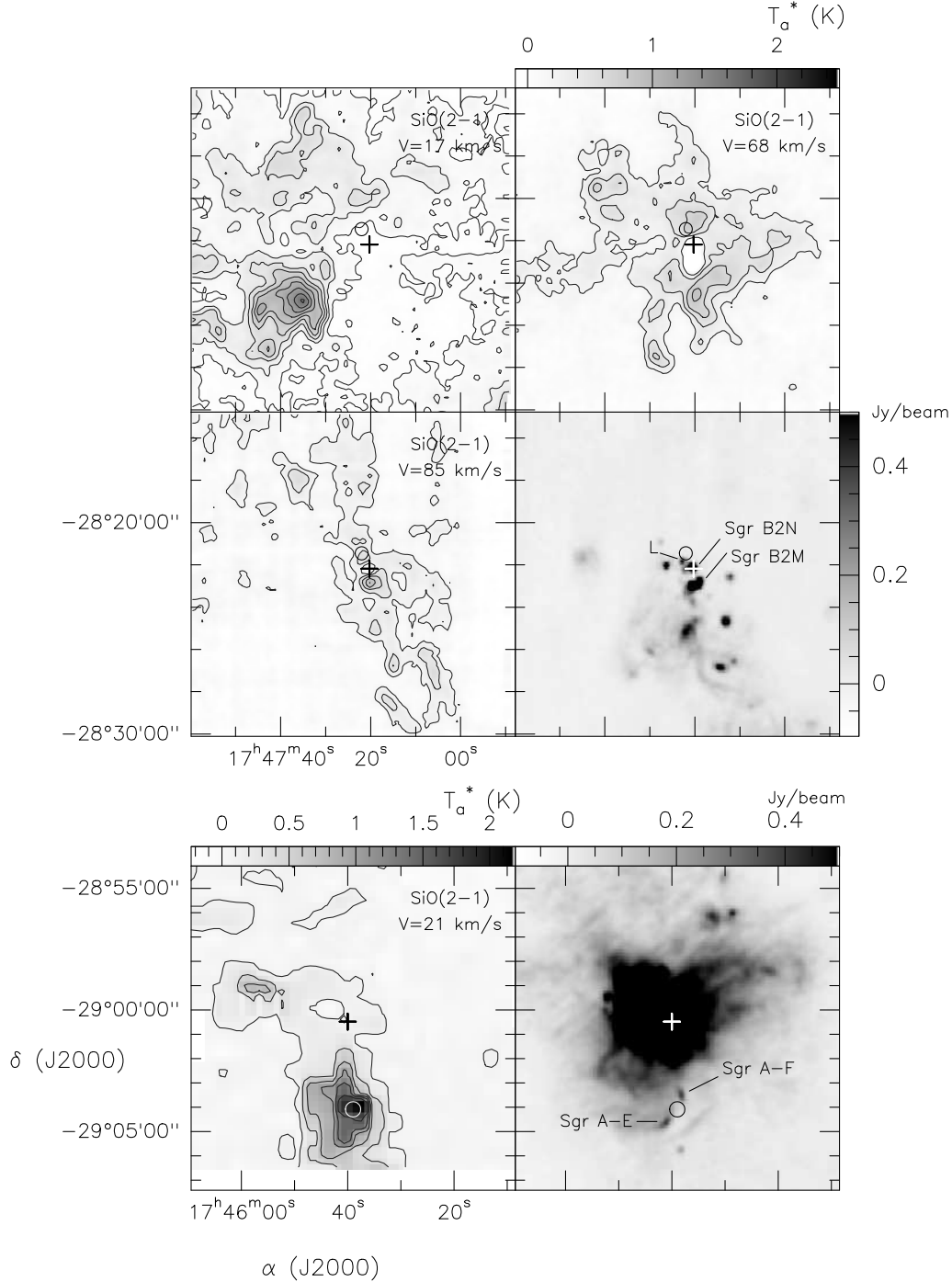


Figure 1. (Upper and middle panels) From left to right and top to bottom, SiO(2-1) large scale emission (Martín-Pintado, priv. communication) maps for velocities of 17, 68 and 85 km s⁻¹ and 20 cm radio continuum map (Yusef-Zadeh et al. 2004) of the Sgr B2 complex. $LOS+0.693$ is shown as a circle with the size of the Mopra telescope beam ($38''$ at 90 GHz) on the SiO(2-1) and 20 cm radio continuum maps. The crosses indicate the position of the massive hot core Sgr B2N on the four maps. The position of the HII region L is indicated on the 20 cm radio continuum map. **(Bottom panels)** From left to right, SiO(2-1) large scale emission (Amo-Baladrón, priv. communication) map for the velocity of 21 km s⁻¹ and 20 cm radio continuum map (Yusef-Zadeh et al. 2004) of the Sgr A complex. $LOS-0.11$ is shown as a circle with the size of the Mopra telescope beam on the SiO(2-1) and 20 cm radio continuum maps. The crosses on the two maps show the position of the compact radio source Sgr A* corresponding to the central supermassive black hole. The features Sgr A-E and Sgr A-F are indicated with lines on the 20 cm radio continuum map.

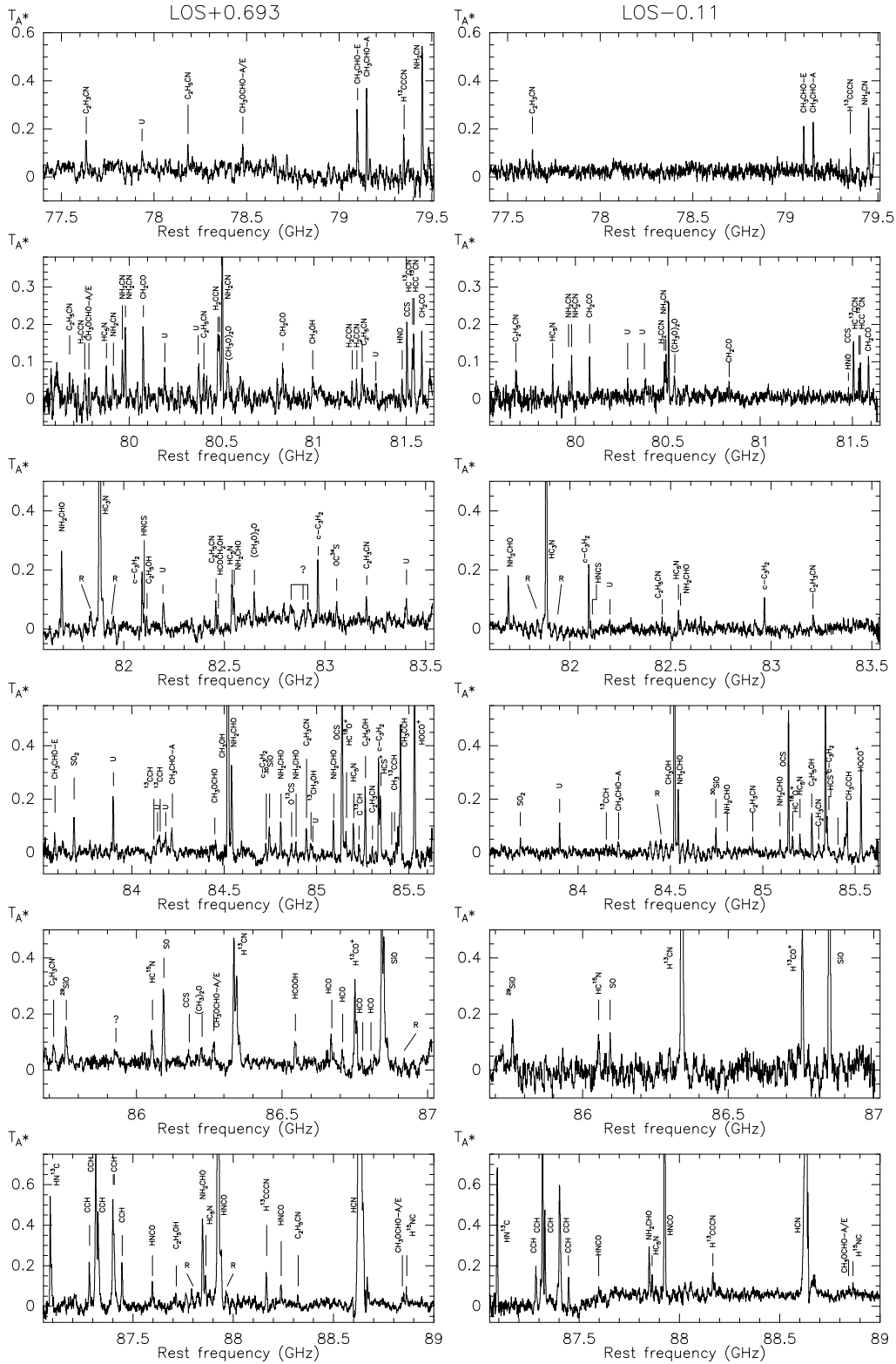
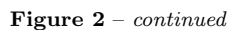


Figure 2. 3 mm spectra of $LOS+0.693$ (left panels) and $LOS-0.11$ (right panels). Each panel shows a spectra with a ~ 2 GHz coverage. Detected transitions of known molecules are indicated, while the unidentified lines are labeled as “U”. Some regions of the spectra affected by ripples are indicated with the letter R.



lines. In contrast, for $LOS-0.11$, we only found 34 molecular species and 18 isotopologues, as well as 8 unidentified lines.

In our survey, we have detected, for the first time, the HCO and HOC^+ emission toward the quiescent gas of $LOS+0.693$ in the GC outside the hot cores of Sgr B2N and Sgr B2M. We have detected four HCO hyperfine lines ($F=2-1$, $1-0$, $1-1$ and $0-1$) and one $HOC^+(1-0)$ line toward $LOS+0.693$ (see Fig. 2 and 3). HCO, HOC^+ , HC_2NC and $HCOCH_2OH$ are not detected toward $LOS-0.11$ (see Fig. 2 and 4). HCO and HOC^+ molecules have been proposed to be tracers of PDRs (Apponi et al. 1999; Goicoechea et al. 2009; Martín et al. 2009b) and XDRs (Usero et al. 2004). Tables 1 and 2 show the line parameters derived by Gaussian fitting to almost all observed molecular lines for both LOS s. The tables also include, for both LOS s, upper limits to the emission of several molecular species, like HOC^+ and HCO, which are relevant for the discussion. These upper limits (4 for $LOS+0.693$ and 16 for $LOS-0.11$) correspond to 3σ of the peak and velocity-integrated intensities (see Tables 1 and 2).

3.2 Line profiles

Most of line profiles from each cloud trace just their kinematic structure, i.e. three velocity components (~ 17 , 68 and 85 km s^{-1}) in $LOS+0.693$ and one velocity component (~ 20 km s^{-1}) in $LOS-0.11$. Additional double-peaked line profiles of certain strong molecular species like HCO^+ , HNC and HCN are likely a result of optical depth effects, as this double-peaked structure is not present in the line profiles of their optically-thin isotopologues. In this paper, we will concentrate on the emission from the 68 and 85 km s^{-1} clouds along $LOS+0.693$ and the ~ 20 km s^{-1} cloud along $LOS-0.11$.

To compare molecular abundances derived from optically-thick lines (e.g. CN, HNC, HCN, HCO^+ and CH_3OH) with those showing simpler profiles we have calculated, in Tables 1 and 2, their velocity-integrated intensities over the selected velocity ranges given in column 4 of these tables. For $LOS+0.693$ we have considered two velocity ranges of 40–80 km s^{-1} and 80–110 km s^{-1} corresponding to the emission of the ~ 68 km s^{-1} and ~ 85 km s^{-1} clouds, respectively. For $LOS-0.11$, we have derived velocity-integrated intensities only for $HCO^+(1-0)$ and HCN(1-0) lines and their corresponding isotopologues.

Fig. 3 and 4 present the line profiles of all detected methanol transitions for $LOS+0.693$ and $LOS-0.11$, respectively. Interestingly the $CH_3OH(3_{1,3}-4_{0,4})$ line is the only methanol line observed in absorption in our survey, while the $CH_3OH(0_{0,0}-1_{-1,1})$ line appears to be optically thick in both LOS s. Furthermore, the $CH_3OH(5_{-1,5}-4_{0,4})$ line at 84.5 GHz is intense and it has been reported to be masing in some sources (Zuckerman et al. 1972; Batrla & Menten 1988).

3.3 Analysis

Assuming optically thin emission and excitation in Local Thermodynamic Equilibrium (LTE), the relation between the LTE total molecular column density N and the measured

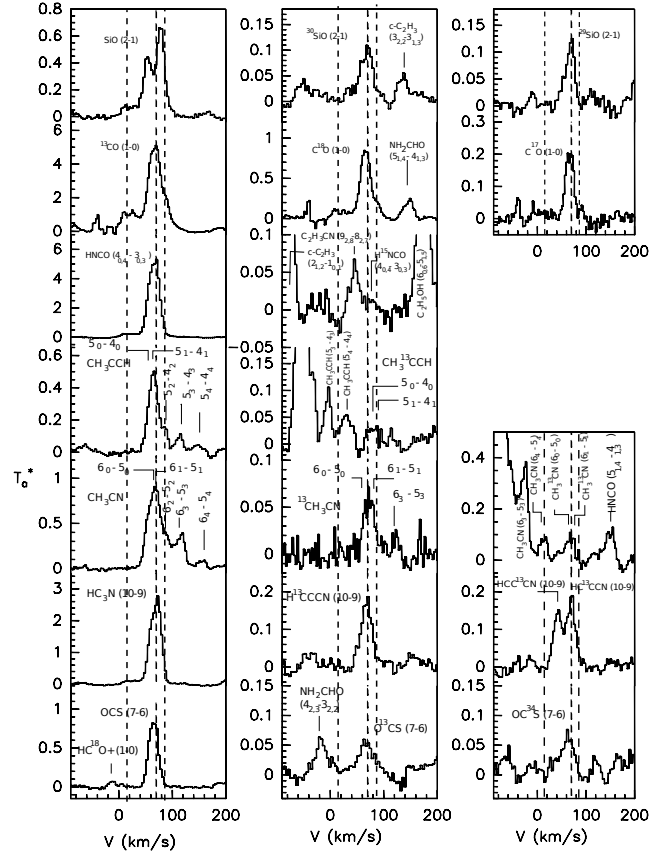


Figure 3. Sample of some molecular lines and their isotopologues observed toward $LOS+0.693$. We used the column densities derived from these transitions and others to estimate the carbon, nitrogen, oxygen, sulfur and silicon isotopic ratios. The vertical dashed lines show the LSR velocities of 17, 68 and 85 km s^{-1} .

integrated line intensity, $W = \int T_A^* dv$ in K km s^{-1} , of a transition is given by:

$$\frac{N_u}{g_u} = \frac{N}{Q_{rot}} e^{-E_u/kT_{rot}} = \frac{1.67 \times 10^{14} W}{\nu \mu^2 S} \quad (1)$$

where N_u is the molecular column density in the upper energy level, g_u and E_u/k are the degeneracy and the energy (in K) of the upper level of the transition with a frequency ν in GHz, a dipole moment μ in Debye and a line strength S . T_{rot} is the LTE rotational temperature in K, Q_{rot} is the rotational partition function. Taking the natural logarithm in (1) we obtain that the main equation of the rotational diagrams (RDs) is given by:

$$\ln \frac{1.67 \times 10^{14} W}{\nu \mu^2 S} = \ln \frac{N}{Q_{rot}} - \frac{E_u}{kT_{rot}}. \quad (2)$$

By observing more than one transition from the same molecule, we can estimate the excitation temperature of the rotational levels, T_{rot} , and the LTE total column densities (by using the Q_{rot} for T_{rot}) from a linear regression fit to equation (2). Since the typical uncertainties of assuming the Rayleigh-Jeans approximation are less than the calibration uncertainties, they are ignored.

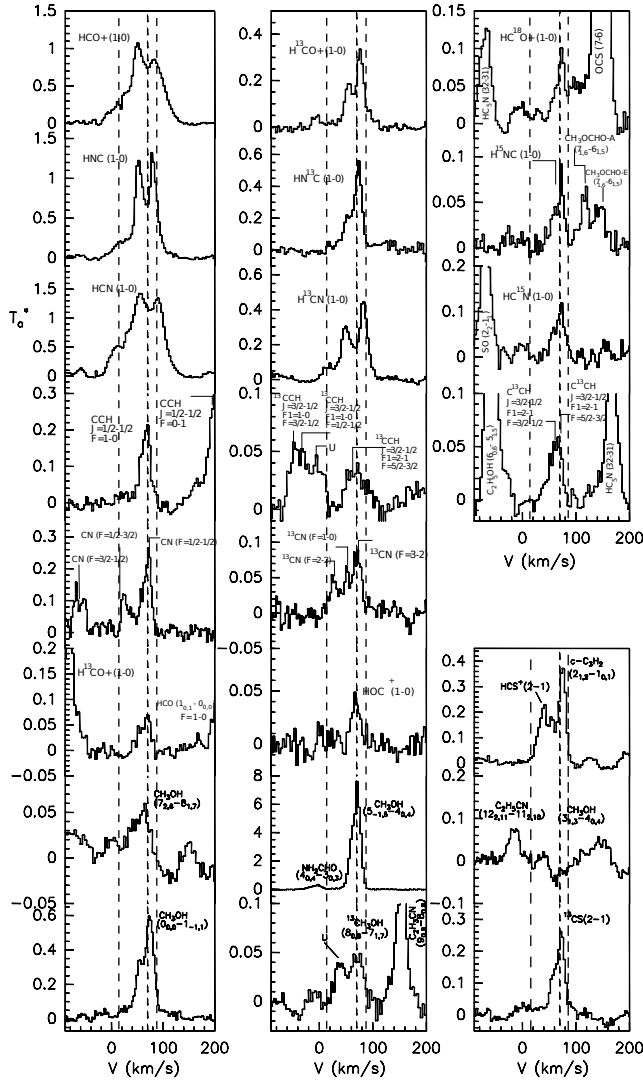


Figure 3 – continued

3.3.1 Rotational temperatures and molecular column densities

We have used the MASSI package with the spectroscopic information (A_{ul} , g_u , E_u , $\mu^2 S$, Q_{rot} , etc) from the JPL and CDMS catalogs to generate the RDs for all molecules with more than one observed transition. Fig. 5 shows RDs (for both GC sources) for selected molecules, and the derived T_{rot} from RDs are listed in Table 3. All RDs are fitted with a single T_{rot} . The uncertainties in the T_{rot} are derived from the 1σ uncertainties in the integrated line intensities and also take into account the uncertainty due to the linear regression fit in the RDs. In our survey, the derived T_{rot} ranges from 5 K to 73 K (see Table 3), however, most of the derived T_{rot} are rather low compared with the estimated mean kinetic temperature of ≈ 100 K found in the GC (Güsten et al. 1985; Hüttemeister et al. 1993), indicating subthermal excitation due to relatively low H_2 densities (see Sec. 3.3.4).

Molecular lines contaminated by the emission from unidentified molecular species (see notes in Tables 1 and 2) were not included in the RDs. When required, we have also properly taken into account the hyperfine structure (see

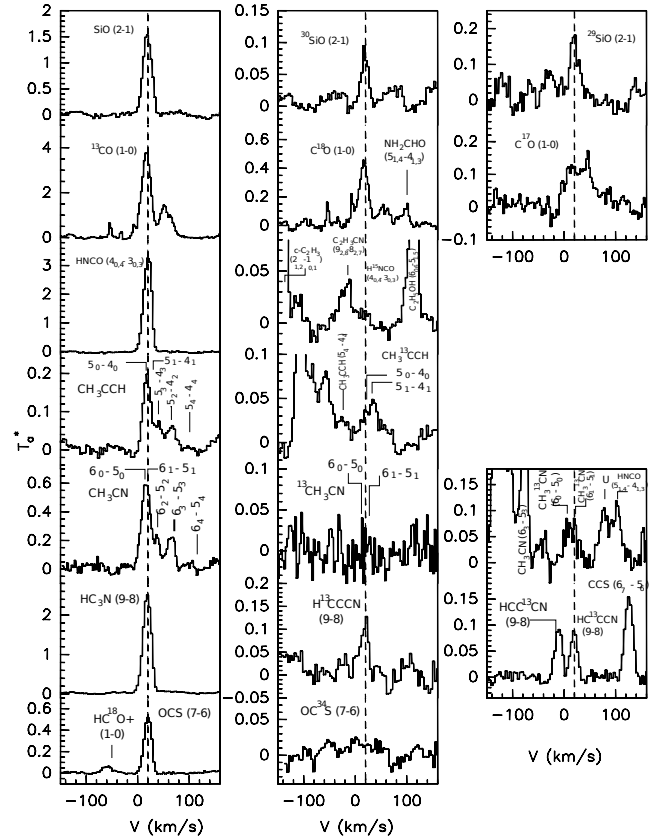


Figure 4. Sample of some molecular lines and their isotopologues observed toward $LOS-0.11$. We used the column densities derived from these transitions and others to estimate the carbon, nitrogen, oxygen, sulfur and silicon isotopic ratios. The vertical dashed line shows the LSR velocity of 20 km s^{-1} .

notes in Tables 1 and 2) to estimate the total column densities given in Table 3. We have used equation (1) to estimate the total column densities for molecules with only one detected transition by assuming a T_{rot} of 10 K, the average value of the low T_{rot} derived from other molecules (see Table 3). We have also used a T_{rot} of 10 K to derive the column densities of molecular species with several observed transitions but with insufficient dynamical range in E_u ($\lesssim 2$ K) to derive a reliable T_{rot} .

To avoid the uncertainties introduced by optical depth effects in the estimated column densities of molecules like HCN, HNC, HCO^+ , in Table 3, when possible, we have derived them from the optically thin lines (see note b in Table 3) of their rarer isotopologues, assuming the typical GC isotopic ratios (Wilson & Rood (1994), hereafter W&R94). The LTE approximation used in our analysis provides beam-averaged abundances which are relatively similar to those obtained by using non-LTE statistical equilibrium methods. The difference in the estimated HC_3N column densities using the LTE and non-LTE analysis is less than a factor of ~ 2 for both GC sources (see Sec. 3.3.4).

To derive the CH_3OH column density for $LOS+0.693$ we have used the $7_{2,6}-8_{1,7}$ transition and the T_{rot} of 14 K derived by Requena-Torres et al. (2008). This transition is selected since it shows thermal emission, is likely optically thin, and is observed in emission toward $LOS+0.693$ (see

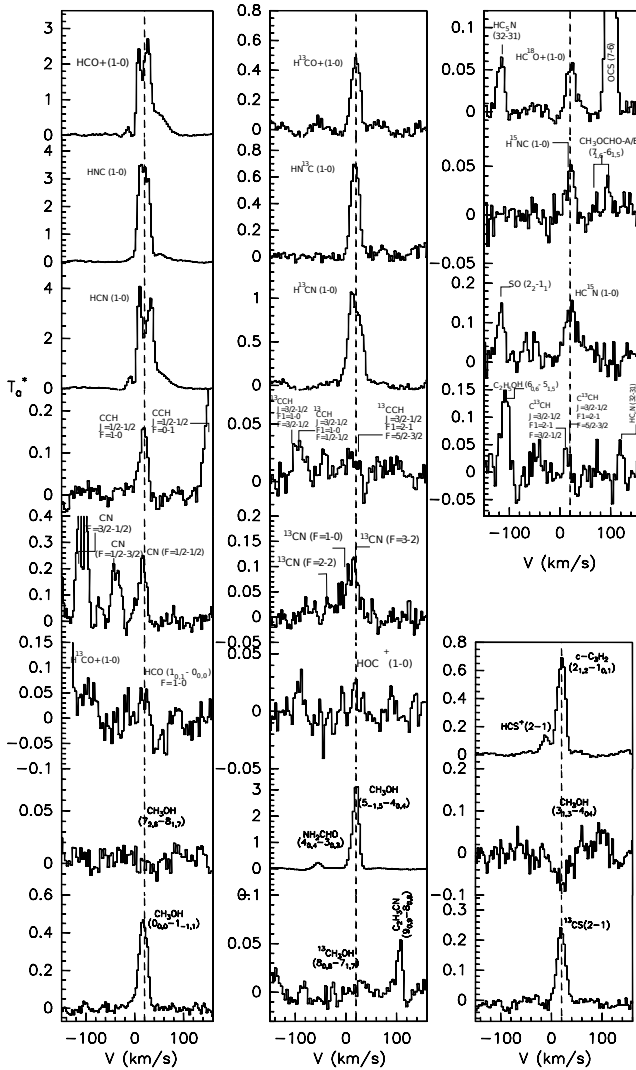


Figure 4 – continued

Sec. 3.2). For $LOS-0.11$ this methanol transition is not detected, so we have derived only an upper limit to the methanol column density by assuming the T_{rot} of 13 K derived by Requena-Torres et al. (2008).

3.3.2 H_2 column densities and molecular abundances

To estimate the molecular fractional abundances relative to H_2 we need to estimate the H_2 column density (N_{H_2}) toward both LOS s. We have used the $C^{18}O$ lines to estimate the H_2 column densities by assuming a $^{16}O/^{18}O$ isotopic ratio of 250 (W&R94) and a relative abundance of CO to H_2 of 10^{-4} (Frerking et al. 1982). We found N_{H_2} of $5.9 (0.2) \times 10^{22} \text{ cm}^{-2}$ and $2.4 (0.2) \times 10^{22} \text{ cm}^{-2}$ for $LOS+0.693$ and $LOS-0.11$, respectively. The estimated relative abundances obtained by dividing the molecular column densities by their respective N_{H_2} are shown in Table 3 for the molecules and velocity components identified in our spectral line survey. Fig. 6 summarizes the derived fractional abundances from Table 3 for all species except for $^{13}C^{15}N$ (its 1-0 transition is contaminated by emission from an unknown molecular species), $O^{13}C^{34}S$ (there is no lower limit for $LOS-0.11$) and HCO^+ , HCN,

HNC and their ^{13}C isotopologues, whose abundances are obtained from their less abundant isotopologues.

It is remarkable, that two LOS s separated by more than ~ 120 pc in the GC show very similar abundances, within a factor of 2, of $\sim 80\%$ of the detected molecular species, including the most complex organic molecules like C_2H_5OH , C_2H_5CN and $(CH_3)_2O$ (see Fig. 6). This finding will be discussed in detail in section 4.1.1.

3.3.3 Kinetic temperatures

Symmetric rotors are usually used to estimate the kinetic temperature, T_{kin} , of the molecular clouds because the radiative transitions between levels of ladders with $\Delta K \neq 0$ are forbidden (Turner 1991), and their excitation is dominated by collisions with H_2 . In our survey we have detected transitions from CH_3CN , $^{13}CH_3CN$, $CH_3^{13}CN$, CH_3CCH and $CH_3^{13}CCH$. We have derived the T_{rot} for both LOS s from the RDs of the 6_K-5_K ($K=0, 1, 2, 3$ and 4) transitions of CH_3CN and the 6_K-5_K ($K=0, 1, 2$ and 3) transitions of CH_3CCH . In addition for $LOS+0.693$ we have also used the 6_K-5_K ($K=0, 1$ and 3) transitions of $^{13}CH_3CN$ (the $K=2$ line is not used because it is blended with the $K=0$ and 1 lines).

As expected, the symmetric rotors CH_3CN , CH_3CCH and $^{13}CH_3CN$ show the highest T_{rot} of $\approx 55-73$ K for both GC sources (see Table 3), indicating that the T_{kin} must be larger than 73 K. For a T_{kin} of 100 K, statistical equilibrium calculations reveal that T_{rot} derived from CH_3CN transitions with $\Delta K \neq 0$ ($K < 4$) approach the T_{kin} only at H_2 densities of $\sim 10^6 \text{ cm}^{-3}$. For H_2 densities of $\lesssim 10^5 \text{ cm}^{-3}$ and a T_{kin} of 100 K, these CH_3CN transitions show T_{rot} of $\lesssim 70$ K (Churchwell et al. 1992). Our results are consistent with the mean T_{kin} of ≈ 100 K derived by Güsten et al. (1985), Hüttemeister et al. (1993) and Rodríguez-Fernández et al. (2001) toward molecular clouds distributed over the central 500 pc of the GC. Thus, for the low H_2 densities ($\sim 10^4 \text{ cm}^{-3}$, see Sec. 3.3.4) found in both GC sources we will consider in the following discussions a T_{kin} of ≈ 100 K.

3.3.4 H_2 densities

We have used the non-LTE excitation and radiative transfer code RADEX with the Large Velocity Gradient (LVG) approximation (van der Tak et al. 2007) to estimate the H_2 densities by using three HC_3N lines (see Tables 1 and 2). For a T_{kin} of 100 K, a linewidth of 21 km s^{-1} , a background temperature of 2.73 K and a beam filling factor of 1 (since the cloud size is much larger than the telescope beam size, see Fig. 1), we have estimated H_2 densities of $\sim 2.3 (0.3) \times 10^4 \text{ cm}^{-3}$ for both GC sources.

The HC_3N column densities and H_2 densities were considered free parameters for the modelling. Our non-LTE analysis provided estimates of the HC_3N column densities of $6.0 \times 10^{14} \text{ cm}^{-2}$ for $LOS+0.693$ and $4.9 \times 10^{14} \text{ cm}^{-2}$ for $LOS-0.11$, in good agreement within a factor of 2 with the LTE calculations of the HC_3N column densities (see Table 3). Our estimated line optical depths are ~ 0.5 for the three HC_3N lines. The predicted excitation temperatures of ~ 14 K are also consistent with the LTE analysis and our assumption of subthermal excitation. Changes in the T_{kin} to lower

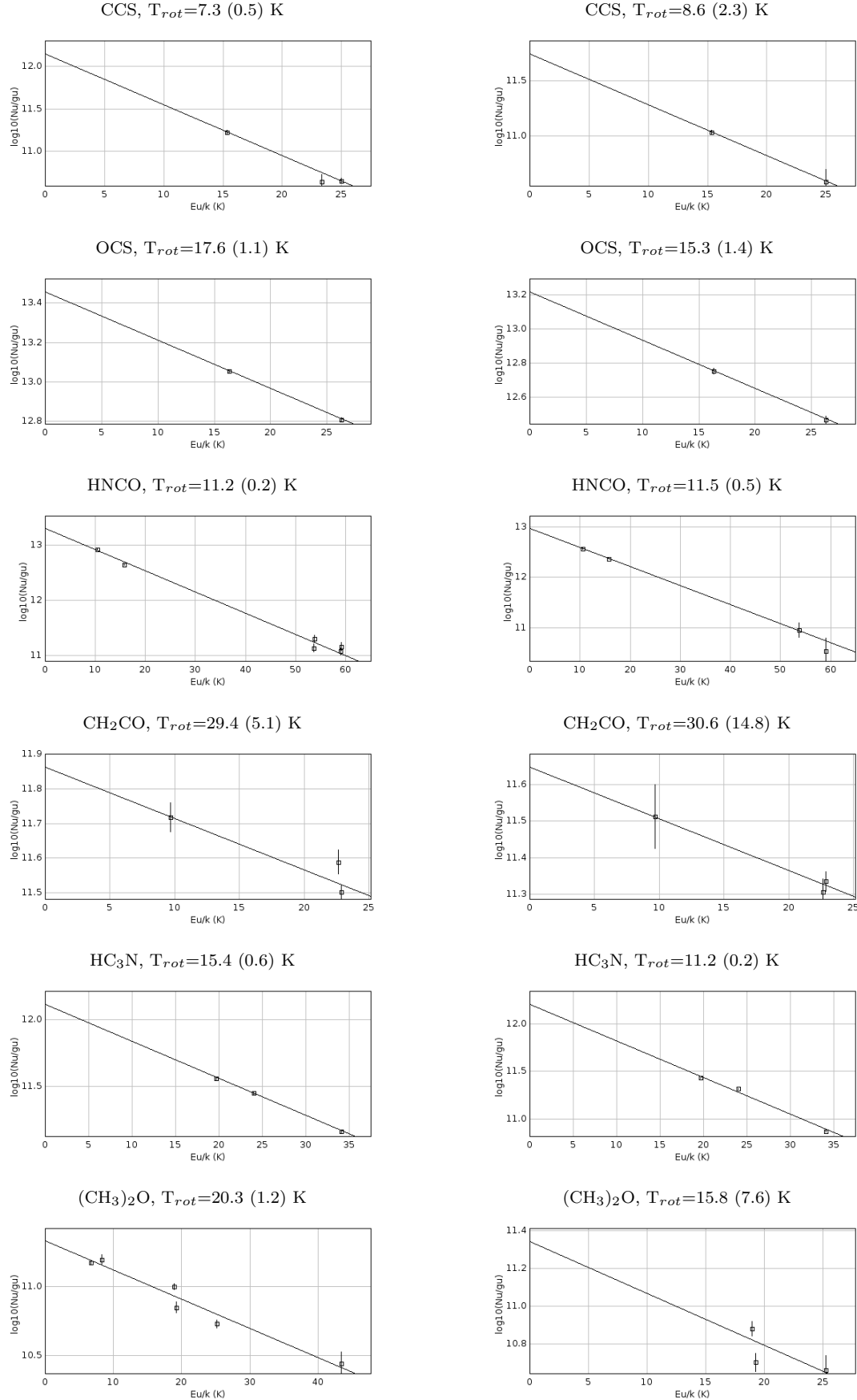


Figure 5. Rotational diagrams of some molecules for $LOS+0.693$ (left panels) and $LOS-0.11$ (right panels).

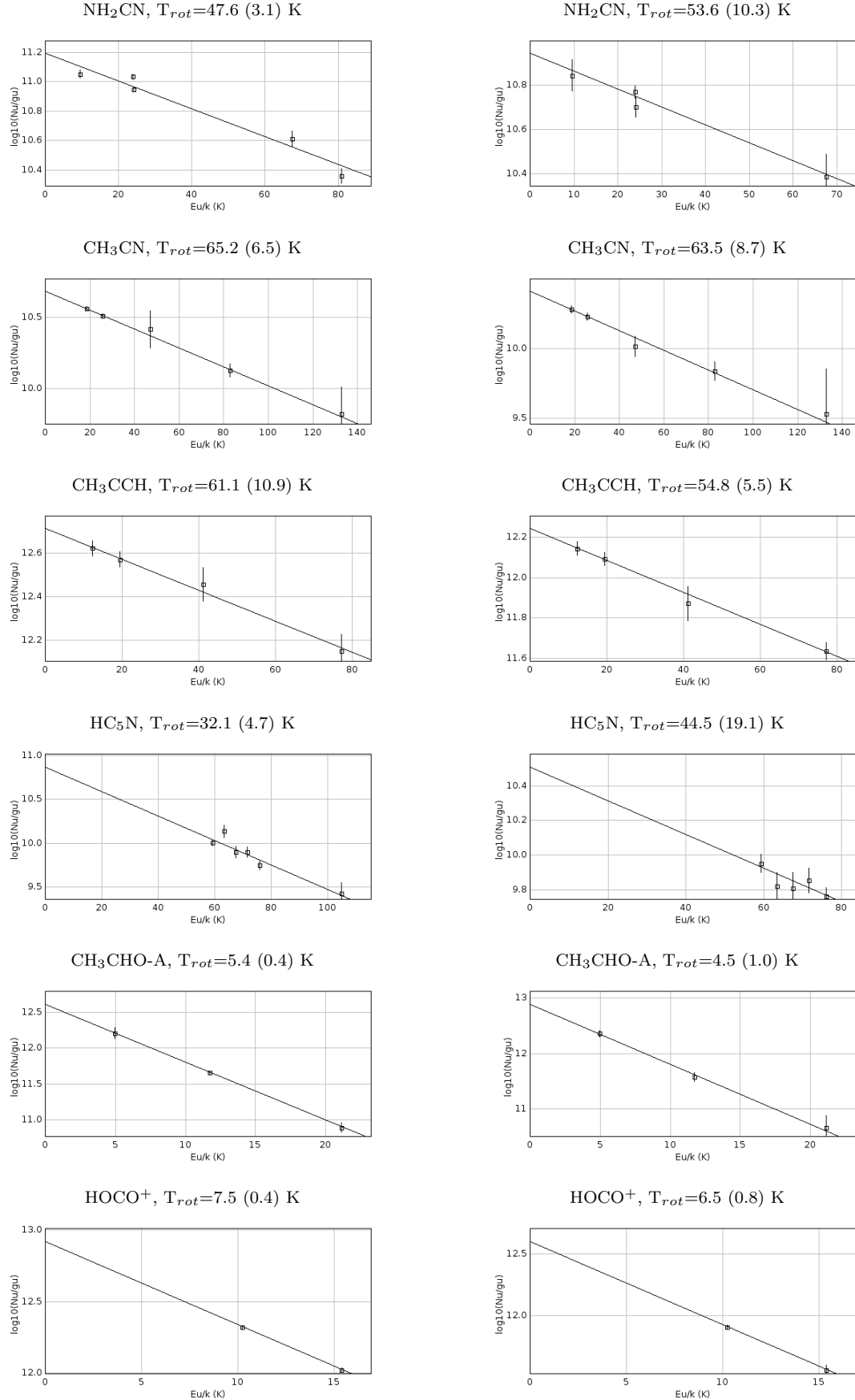


Figure 5 – continued

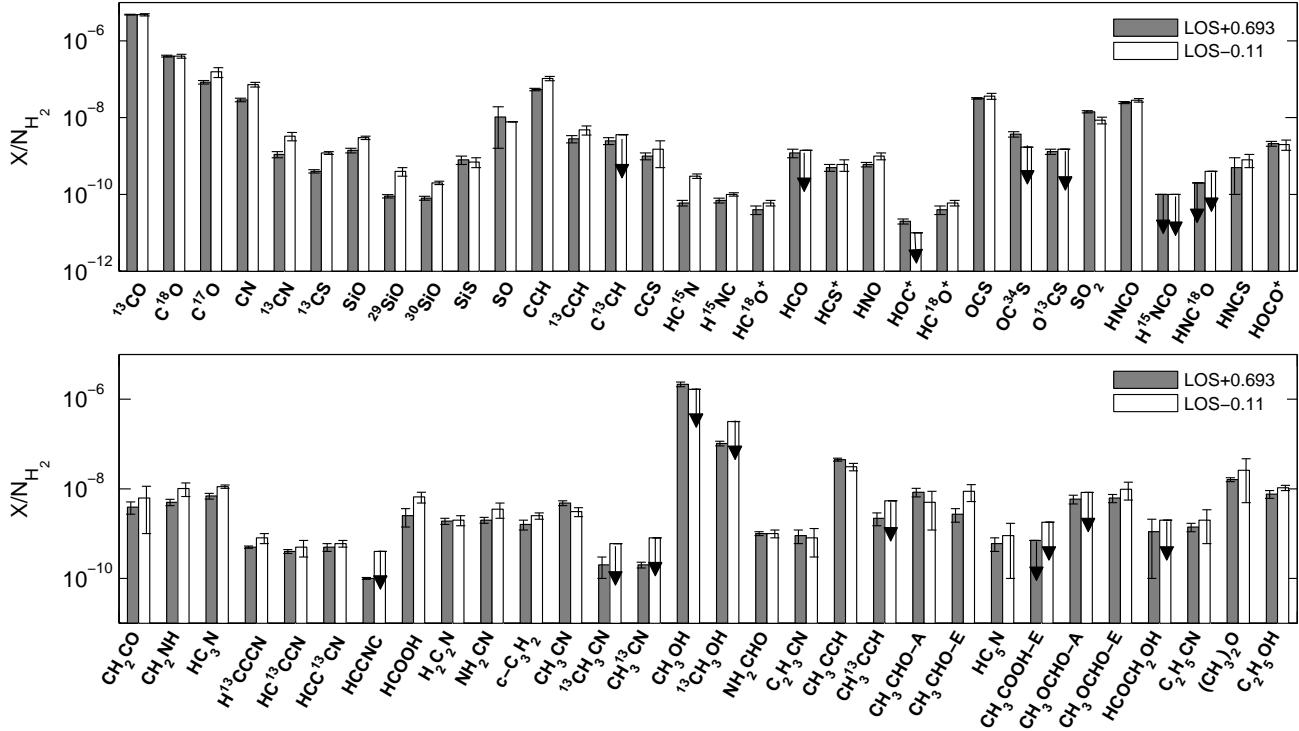


Figure 6. Abundances relative to H_2 for molecules detected in this survey. Arrows correspond to upper limits to the derived abundances. CH_3OH lines are observed in $LOS-0.11$, but we were only able to derive an upper limit to the CH_3OH column density (see Sec. 3.3.1).

values of ~ 50 K, will increase the H_2 densities by only a factor of 2, to $\sim 5 \times 10^4 \text{ cm}^{-3}$. The derived excitation temperatures are very sensitive to the H_2 density. Changes in a factor of 2 in the H_2 densities increase the excitation temperature from ~ 14 K to ~ 24 K. The latter predicted temperature is inconsistent with our measured T_{rot} for HC_3N , ruling out higher H_2 densities in both GC sources.

3.4 Isotopic ratios

We have used the large number of detected isotopologues to derive from their column densities the isotopic ratios of $^{12}C/^{13}C$, $^{14}N/^{15}N$, $^{16}O/^{18}O$, $^{18}O/^{17}O$, $^{29}Si/^{30}Si$ and $^{32}S/^{34}S$ for both GC sources. Table 4 summarizes all the derived isotopic ratios based on optically thin (unbiased group) and optically thick (biased group) emission. When possible, we have also used column densities of isotopologues with double isotopic substitution to guarantee optically thin emission. The canonical isotopic ratios derived for the GC by W&R94 are also shown in Table 4. As expected, the isotopic ratios of ~ 3 -15 derived from the biased group are always smaller than the canonical isotopic ratios due to the opacity effects on the most abundant isotopic substitution. The unbiased $^{12}C/^{13}C$ isotopic ratios derived for both GC sources are similar, within uncertainties, and its average, $^{12}C/^{13}C = 21.3$ (1.7), is similar to the canonical value.

We also found a $^{18}O/^{17}O$ ratio of 3.7 (0.5) and a $^{29}Si/^{30}Si$ ratio of 1.7 (0.2) averaged over both GC sources, which are also within the uncertainties similar to the canonical values. Our lower limits to the $^{16}O/^{18}O$ and $^{14}N/^{15}N$

ratios are also consistent with the canonical values. The $^{32}S/^{34}S$ isotopic ratios derived in $LOS+0.693$ are lower than that found in W&R94, because the $OC^{34}S$ lines are affected by ripples (see Fig. 2) and likely the $OC^{34}S$ column density is overestimated. However, in $LOS-0.11$ the lower limit of 22 to the $OCS/OC^{34}S$ ratio is close to the canonical value. Our averaged $^{12}C/^{13}C$, $^{18}O/^{17}O$, $^{29}Si/^{30}Si$ isotopic ratios are similar to the canonical values (W&R94) within 1σ , which represents $\sim 10\%$ in the derived isotopic ratios. This indicates that chemical isotopic fractionation and selective photodissociation are negligible, less than $\sim 10\%$, for most of the molecules and the physical conditions in the GC, consistent with the results obtained by Riquelme et al. (2010).

The ^{12}C isotope is a primary product of nucleosynthesis in stellar cores, while the ^{13}C isotope is thought to be formed from ^{12}C present in stars of later generations (Wilson & Matteucci 1992). Thus, the $^{12}C/^{13}C$ ratio can be considered a measure of the degree of gas processing in the ISM. Using CCH and their ^{13}C isotopologues, Martín et al. (2010) derived very large $^{12}C/^{13}C$ ratios of >138 and >81 toward the starburst galaxies M 82 and NGC 253, respectively. Based on the hyperfine fits to the CCH line profiles, they ruled out opacity effects in the CCH lines. The $^{12}C/^{13}C$ ratio in the GC is at least a factor of 4 lower than in both starburst galaxies, suggesting that the degree of gas processing is quite different between them.

Table 1. Line parameters for *LOS*+0.693.

Molecule	Frequency (MHz)	Transition	Area (σ) (K km s ⁻¹)	V _{LSR} (σ) (km s ⁻¹)	$\Delta v_{1/2}$ (σ) (km s ⁻¹)	T* _A (σ) (mK)	Notes
C ₂ H ₃ CN	77633.8	8 _{1,7} -7 _{1,6}	2.6 (0.5)	63.9 (1.4)	19.6 (3.2)	125.8 (15.6)	
Unidentified	77935.5		2.9 (1.1)	65.0 (5.0)	25.0 (5.0)	88.1 (18.2)	
C ₂ H ₅ CN	78183.6	9 _{1,9} -8 _{1,8}	3.6 (0.6)	64.2 (1.5)	30.5 (3.5)	111.0 (11.9)	
CH ₃ OCHO ^c	78481.3	7 _{1,7} -6 _{1,6} A+E	1.7 (0.4)	71.7 (1.4)	24.8 (2.7)	129.5 (7.6)	bl
CH ₃ CHO	79099.3	4 _{1,3} -3 _{1,2} E	5.6 (0.4)	70.5 (0.4)	20.7 (1.0)	0.3 (11.6)	
CH ₃ CHO	79150.2	4 _{1,3} -3 _{1,2} A	10.0 (0.6)	70.9 (0.4)	22.5 (1.0)	418.0 ^a (16.1)	
H ¹³ CCCN	79350.4	9 _K -8 _K , K=8-7, 9-8, 10-9	4.9 (0.3)	70.5 (0.5)	22.8 (1.3)	202.6 (8.8)	hf
NH ₂ CN	79449.7	4 _{1,4} -3 _{1,3}	10.9 (0.5)	68.4 (0.3)	19.2 (0.7)	534.9 (14.2)	
C ₂ H ₅ CN	79677.5	9 _{0,9} -8 _{0,8}	2.6 (0.5)	64.3 (1.9)	29.2 (4.5)	83.8 (11.5)	
H ₂ C ₂ N	79759.4	4 _{1,4} -3 _{1,3} , J=9/2-7/2	2.1 (0.5)	65.9 ^a (1.7)	19.1 ^a (3.9)	103.7 (7.3)	hf ^a
CH ₃ OCHO ^c	79783.8	7 _{0,7} -6 _{0,6} A+E	1.6 (0.3)	75.7 (0.7)	25.4 (1.7)	115.9 (6.1)	bl
HC ₅ N	79876.9	30-29	2.8 (0.2)	67.4 (0.6)	22.4 (1.4)	115.5 (6.4)	
NH ₂ CN	79915.1	4 _{0,4} -3 _{0,3}	1.8 (0.2)	72.9 (0.8)	24.0 (2.0)	68.2 (5.1)	
NH ₂ CN	79963.2	4 _{2,3} -3 _{2,2}	1.1 (0.1)	63.7 (0.7)	19.0 (1.5)	109.9 (7.8)	m
NH ₂ CN	79979.5	4 _{0,4} -3 _{0,3}	4.1 (0.3)	65.1 (0.4)	19.0 (1.0)	200.9 (7.4)	
CH ₂ CO	80076.7	4 _{1,4} -3 _{1,3}	4.2 (0.3)	68.2 (0.6)	20.7 (1.3)	190.8 (9.0)	
Unidentified	80193.2		1.6 (0.4)	65.6 (1.5)	19.0 (3.5)	77.8 (10.4)	
Unidentified	80373.6		2.6 (1.0)	63.6 (3.2)	25.0 (7.8)	86.7 (20.3)	
C ₂ H ₅ CN	80404.9	9 _{2,8} -8 _{2,7}	3.2 (0.4)	68.8 (1.5)	35.0 (3.5)	84.9 (8.2)	
H ₂ C ₂ N	80480.9	4 _{0,4} -3 _{0,3} , J=9/2-7/2	3.9 (0.5)	61.1 ^a (1.1)	21.4 ^a (2.2)	170.7 (10.9)	hf ^a
H ₂ C ₂ N	80489.9	4 _{0,4} -3 _{0,3} , J=7/2-5/2	2.4 (1.6)	68.5 ^a (9.2)	18.9 ^a (10.4)	119.0 ^a (45.5)	hf ^a
NH ₂ CN	80504.6	4 _{1,3} -3 _{1,2}	9.1 (0.3)	65.7 (0.2)	18.9 (0.4)	451.4 (7.4)	
(CH ₃) ₂ O ^b	80538.5	5 _{2,3} -5 _{1,4}	2.6 (0.4)	75.5 ^a (2.4)	28.4 ^a (4.1)	86.0 (6.7)	
CH ₂ CO	80832.1	4 _{0,4} -3 _{0,3}	2.0 (0.2)	65.6 (0.8)	23.8 (1.8)	80.1 (4.9)	
CH ₃ OH	80993.2	7 _{2,6} -8 _{1,7} A-	1.0 (0.2)	62.5 (1.5)	19.0 (3.4)	49.0 (7.0)	cd
H ₂ C ₂ N	81207.3	4 _{1,3} -3 _{1,2} , J=7/2-5/2	1.2 (0.2)	67.2 (0.8)	18.7 (1.9)	60.4 (4.8)	hf ^a
H ₂ C ₂ N	81232.5	4 _{1,3} -3 _{1,2} , J=9/2-7/2	1.3 (0.2)	70.4 (0.7)	18.7 (1.7)	64.2 (4.6)	hf ^a , cd
C ₂ H ₅ CN	81261.3	9 _{2,7} -8 _{2,6}	2.4 (0.5)	65.1 (1.8)	29.2 (4.3)	76.0 ^a (9.2)	
Unidentified	81337.8		1.7 (0.3)	68.3 (1.5)	28.1 (3.4)	57.0 (5.7)	
HNO	81477.4	1 _{0,1} -0 _{0,0}	1.5 (0.2)	67.5 ^a (0.8)	18.7 ^a (2.0)	77.0 (6.1)	hf
CCS	81505.1	6 ₇ -5 ₆	4.8 (0.3)	68.5 (0.4)	19.6 ^a (0.8)	232.1 (7.8)	
HC ¹³ CCN	81534.1	9 _K -8 _K , K=8-7, 9-8, 10-9	4.1 (0.4)	64.5 ^a (1.0)	28.0 (2.0)	137.3 (8.7)	hf
HCC ¹³ CN	81541.9	9 _K -8 _K , K=8-7, 9-8, 10-9	3.8 (0.3)	67.8 (0.6)	23.3 (1.6)	154.2 (5.6)	hf
CH ₂ CO	81586.2	4 _{1,3} -3 _{1,2}	3.5 (0.2)	66.7 (0.4)	21.7 (0.8)	151.1 (4.4)	
NH ₂ CHO	81693.5	4 _{1,4} -3 _{1,3}	6.3 (0.3)	68.0 (0.4)	24.3 (1.0)	245.4 (8.1)	hf
HC ₃ N	81881.4	9-8	67.2 (1.8)	66.7 (0.2)	24.9 (0.5)	2534.8 (43.0)	
c-C ₃ H ₂	82093.5	2 _{0,2} -1 _{1,1}	3.8 (0.4)	71.0 (0.6)	18.5 (1.5)	194.8 (12.1)	
HNCS, a-type	82101.8	7 _{0,7} -6 _{0,6}	1.8 (0.4)	67.8 (1.6)	23.9 (3.9)	70.1 (8.5)	
C ₂ H ₅ OH	82115.7	3 _{2,2} -3 _{1,3}	1.2 (0.3)	71.8 (1.3)	18.7 (3.0)	60.6 (8.4)	
Unidentified	82198.8		2.7 (0.2)	67.9 (0.9)	27.8 (2.0)	90.0 (5.0)	
C ₂ H ₅ CN	82458.5	9 _{1,8} -8 _{1,7}	3.7 (0.3)	67.6 (0.7)	29.2 (1.8)	20.4 (4.7)	
HCOCH ₂ OH	82470.6	8 _{0,8} -7 _{1,7}	1.0 (0.2)	73.8 (0.9)	19.6 (2.3)	47.3 (4.6)	
HC ₅ N	82539.2	31-30	4.0 (0.6)	64.0 (1.4)	27.7 (3.3)	141.5 (14.0)	
NH ₂ CHO	82549.5	1 _{1,1} -0 _{0,0}	2.9 (0.2)	67.0 (0.7)	25.6 (1.8)	108.9 (4.6)	hf, cl
(CH ₃) ₂ O ^b	82650.1	3 _{1,3} -2 _{0,2}	3.6 (0.2)	65.6 (0.6)	27.6 (1.4)	123.0 ^a (4.3)	
O ¹³ C ³⁴ S	82762.5	7-6	≤0.3	≤33	
c-C ₃ H ₂	82966.2	3 _{1,2} -3 _{0,3}	4.2 (0.2)	67.4 (0.3)	18.4 (0.8)	212.5 (7.5)	
OC ³⁴ S	83057.9	7-6	2.1 (0.3)	65.0 (1.3)	27.5 (3.0)	72.4 (6.6)	
HNC ¹⁸ O	83191.5	4 _{0,4} -3 _{0,3}	≤0.1	≤39	hf
C ₂ H ₃ CN	83207.5	9 _{1,9} -8 _{1,8}	2.2 (0.1)	70.1 (0.5)	20.4 (1.1)	98.7 (3.9)	
Unidentified	83404.9		2.0 (0.3)	68.7 (1.2)	27.4 (2.7)	69.0 (5.4)	
CH ₃ CHO	83584.2	2 _{-1,2} -1 _{0,1} E	2.1 (0.4)	68.9 (1.2)	18.2 (3.1)	0.1 ^a (10.6)	
SO ₂	83688.0	8 _{1,7} -8 _{0,8}	4.2 (0.2)	65.0 (0.4)	25.9 (0.8)	153.0 (4.1)	
Unidentified	83900.3		5.2 (0.4)	65.4 (0.6)	24.2 (1.4)	202.7 (9.3)	
¹³ CCH	84119.3	N=1-0, F ₁ =2-1, F=5/2-3/2	1.2 (0.3)	67.6 (2.4)	36.2 (5.7)	32.0 (4.1)	hf, cd
Unidentified	84139.0		0.7 (0.3)	67.6 (2.4)	18.1 (5.8)	37.3 (8.2)	
¹³ CCH	84153.3	N=1-0, F ₁ =1-0, F=3/2-1/2	2.1 (0.5)	84.5 (2.6)	36.2 (6.1)	55.1 (7.2)	hf
Unidentified	84183.9		1.2 (0.3)	65.2 (1.4)	18.1 (3.3)	60.0 (8.9)	
CH ₃ CHO	84219.7	2 _{1,2} -1 _{0,1} A	2.7 (0.5)	74.8 (1.5)	29.0 (3.6)	88.6 (10.1)	
CH ₃ OCHO	84449.1	7 _{2,6} -6 _{2,5} E	0.9 (0.3)	69.5 ^a (1.7)	18.0 (4.0)	48.0 (8.4)	
CH ₃ OCHO	84454.7	7 _{2,6} -6 _{2,5} A	1.3 (0.3)	66.0 (1.3)	18.0 (3.3)	69.0 (6.4)	
CH ₃ OH	84521.1	5 _{-1,5} -4 _{0,4} E	128.0 (5.1)	68.5 (0.2)	18.0 (0.6)	6678.0 ^a (164.6)	
NH ₂ CHO	84542.4	4 _{0,4} -3 _{0,3}	7.3 (0.5)	71.4 (0.6)	24.4 (1.3)	280.2 (11.8)	hf
c-C ₃ H ₂	84727.6	3 _{2,2} -3 _{1,3}	0.8 (0.2)	67.3 (1.4)	19.8 (3.2)	38.8 (4.8)	
³⁰ SiO	84745.9	2-1	2.2 (0.2)	71.8 (0.6)	18.0 (1.4)	116.0 ^a (6.0)	
NH ₂ CHO	84807.9	4 _{2,3} -3 _{2,2}	2.6 (0.2)	69.0 (0.4)	20.9 (1.0)	116.7 (4.3)	hf
O ¹³ CS	84865.1	7-6	0.9 (0.1)	65.8 (0.9)	17.9 (2.1)	45.0 ^a (3.8)	
NH ₂ CHO	84888.9	4 _{3,2} -3 _{3,1}	1.1 (0.1)	67.5 (0.8)	17.9 (1.9)	56.3 (4.6)	hf, bl
C ₂ H ₃ CN	84946.0	9 _{0,9} -8 _{0,8}	2.6 (0.2)	67.6 (0.7)	25.8 (1.7)	93.7 (4.6)	
¹³ CH ₃ OH	84970.2	8 _{0,8} -7 _{1,7} A+	1.5 (0.3)	70.4 (1.9)	26.9 (4.3)	52.1 (4.6)	
Unidentified	84980.0		1.0 (0.2)	67.9 (2.5)	23.7 (5.0)	37.0 (6.0)	
NH ₂ CHO	85093.3	4 _{2,2} -3 _{2,1}	3.3 (0.3)	67.6 (0.7)	23.0 (1.5)	136(7.6)	hf
OCS	85139.1	7-6	20.7 (0.5)	64.6 (0.2)	22.2(0.4)	876.7(12.7)	
HC ¹⁸ O ⁺	85162.1	1-0	2.0 (0.8)	74.5 (2.8)	17.9 (7.1)	104.0 (7.6)	
HC ₅ N	85201.6	32-31	2.4 (0.4)	67.3 (1.1)	21.7 (2.6)	105.3 (10.0)	
C ¹³ CH	85229.3	N=1-0, F ₁ =2-1 F=5/2-3/2	2.0 (0.3)	60.6 (1.5)	26.8 (3.6)	68.9 (7.3)	hf
C ₂ H ₅ OH	85265.5	6 _{0,6} -5 _{1,5}	7.2 (0.3)	64.5 (0.3)	23.9 (0.8)	282.9 (7.3)	cl
H ¹⁵ NCO	85292.1	4 _{0,4} -3 _{0,3}	≤0.3	≤36	

Table 1 – continued

Molecule	Frequency (MHz)	Transition	Area (σ) (K km s ⁻¹)	V _{LSR} (σ) (km s ⁻¹)	$\Delta v_{1/2}$ (σ) (km s ⁻¹)	T* _A (σ) (mK)	Notes
C ₂ H ₃ CN	85302.6	9 _{2,8} -8 _{2,7}	1.4 (0.3)	68.5 ^a (1.8)	17.8 (3.6)	72.1 (5.6)	
c-C ₃ H ₂	85338.8	2 _{1,2} -1 _{0,1}	8.9 (0.4)	[40, 80]	
			1.6 (0.4)	[80, 110]	
HCS ⁺	85347.9	2-1	5.2 (0.6)	70.4 (0.7)	17.8 (1.8)	275.0 ^a (10.4)	bl
CH ₃ ¹³ CCH	85407.2	5 ₃ -4 ₃	0.4 (0.2)	65.8 (1.7)	8.9 (4.1)	41.8 (9.0)	
CH ₃ ¹³ CCH	85421.8	5 _K -4 _K , K=0, 1	0.7 (0.2)	80.9 (2.2)	17.8 (5.2)	36.6 (6.9)	m, cd
CH ₃ CCH	85442.5	5 ₃ -4 ₃	2.6 (0.5)	68.5 ^a (1.1)	17.8 (2.7)	137.3 (13.7)	
CH ₃ CCH	85450.7	5 ₂ -4 ₂	3.5 (0.6)	69.5 ^a (1.0)	17.8 (2.7)	183.0 ^a (16.1)	bl
CH ₃ CCH	85457.2	5 _K -4 _K , K=0, 1	11.2 (0.9)	66.5 (0.5)	20.8 (1.4)	508.6 (25.1)	m
HOCO ⁺	85531.5	4 _{0,4} -3 _{0,3}	17.3 (0.4)	64.8 (0.2)	22.1 (0.4)	737.4 (10.4)	
C ₂ H ₃ CN	85715.4	9 _{2,7} -8 _{2,6}	1.0 (0.2)	67.4 (1.5)	15.7 (3.6)	56.4 (6.1)	
²⁹ SiO	85759.0	2-1	2.4 (0.2)	65.6 (0.6)	17.8 (1.3)	129.0 ^a (6.9)	
HC ¹⁵ N	86054.9	1-0	1.8 (0.2)	[40, 80]	
			1.0 (0.2)	[80, 110]	
SO	86093.9	2 ₂ -1 ₁	8.0 (0.4)	67.6 (0.5)	26.6 (1.1)	288.0 (10.1)	
CCS	86181.3	7 ₆ -6 ₅	1.1 (0.2)	71.9 (1.4)	19.6 ^a (3.3)	54.0 ^a (5.7)	
(CH ₃) ₂ O ^b	86226.7	2 _{2,0} -2 _{1,1}	1.7 (0.3)	76.7 (1.2)	26.5 (3.5)	60.6 (5.1)	bl
CH ₃ OCHO ^c	86265.8	7 _{3,5} -6 _{3,4} A+E	0.8 (0.2)	62.9 (1.0)	17.6 (2.2)	84.0 ^a (7.2)	bl
H ¹³ CN	86340.1	1-0, F=1-1, 2-1, 0-1	9.1 (0.1)	[40,80]	hf
			6.3 (0.1)	[80,110]	
HCOOH	86546.1	4 _{1,4} -3 _{1,3}	1.9 (0.3)	68.5 ^a (0.8)	17.6 (2.0)	102.9 (7.4)	
HCO	86670.7	1 _{0,1} -0 _{0,0} , J=3/2-1/2, F=2-1	2.0 (0.3)	69.4 (0.9)	17.6 ^a (2.2)	108.4 (9.8)	hf ^a
HCO	86708.3	1 _{0,1} -0 _{0,0} , J=3/2-1/2, F=1-0	1.7 (0.3)	68.5 ^a (1.3)	17.6 ^a (3.0)	89.0 ^a (10.0)	hf ^a , cd
H ¹³ CO ⁺	86754.2	1-0	7.3 (0.1)	[40, 80]	
			3.5 (0.1)	[80, 110]	
HCO	86777.4	1 _{0,1} -0 _{0,0} , J=1/2-1/2, F=1-1	1.0 (0.3)	75.0 (1.6)	17.5 (3.8)	54.7 (9.5)	hf ^a
HCO	86805.7	1 _{0,1} -0 _{0,0} , J=1/2-1/2, F=0-1	0.7 (0.2)	67.9 (1.4)	14.9 (3.7)	45.5 (7.0)	hf ^a
SiO	86846.9	2-1	13.9 (0.4)	[40,80]	
			6.4 (0.4)	[80,110]	
HN ¹³ C	87090.8	1-0	11.1 (0.2)	[40, 80]	
			0.1 (0.2)	[80, 110]	
CCH	87284.1	N=1-0, J=3/2-1/2, F=1-1	3.4 (0.5)	67.2 (0.9)	17.8 (2.1)	181.4 (18.1)	hf ^a
CCH	87316.9	N=1-0, J=3/2-1/2, F=2-1	19.1 (0.8)	69.1 (0.4)	26.0 (0.9)	689.0 ^a (14.9)	hf ^a
CCH	87328.6	N=1-0, J=3/2-1/2, F=1-0	6.8 (0.8)	70.3 (0.8)	17.4 ^a (2.0)	367.3 (15.0)	hf ^a
CCH	87402.0	N=1-0, J=1/2-1/2, F=1-1	7.8 (0.5)	69.5 (0.5)	16.1 (0.9)	455.2 (19.4)	hf ^a , bl
CCH	87407.1	N=1-0, J=1/2-1/2, F=0-1	6.6 (0.5)	66.8 (0.7)	23.2 (1.5)	266.5 (9.2)	hf ^a , bl
CCH	87446.5	N=1-0, J=1/2-1/2, F=1-0	4.5 (0.3)	65.4 (0.4)	20.1 (0.9)	211.0 (8.3)	hf ^a , cd
HNCO	87597.3	4 _{1,4} -3 _{1,3}	2.1 (0.4)	66.6 (1.0)	17.4 (2.4)	113.0 ^a (10.9)	hf
C ₂ H ₅ OH	87716.1	5 _{2,4} -5 _{1,5}	1.1 (0.2)	66.6 (1.2)	18.8 (2.9)	53.7 (7.1)	
NH ₂ CHO	87848.9	4 _{1,3} -3 _{1,2}	11.5 (1.1)	67.8 (0.8)	26.7 (1.9)	405.4 (26.2)	hf
HC ₅ N	87863.9	33-32	2.6 (0.3)	69.5 (1.0)	22.2 (2.3)	109.0 (8.2)	
HNCO	87925.2	4 _{0,4} -3 _{0,3}	140.2 (3.2)	66.1 (0.2)	24.6 (0.4)	5355.9 (78.9)	hf
H ¹³ CCCN	88166.8	10 _K -9 _K , K=10-9, 11-10, 9-8	4.1 (0.3)	67.5 (0.5)	23.6 (1.1)	162.8 (6.3)	hf
HNCO	88239.0	4 _{1,3} -3 _{1,2}	3.1 (0.4)	65.9 (1.2)	25.9 (3.1)	113.6 (8.5)	hf
C ₂ H ₅ CN	88323.7	10 _{0,10} -9 _{0,9}	1.7 (0.3)	68.7 (1.1)	22.9 (2.6)	69.0 ^a (7.1)	
HCN	88631.8	1-0, F=0-1, 1-1, 2-1	53.9 (0.2)	[40,80]	hf
			34.2 (0.2)	[80,110]	
CH ₃ OCHO	88843.2	7 _{1,6} -6 _{1,5} E	0.6 (0.2)	70.1 (2.5)	17.1 (6.1)	30.0 ^a (7.7)	
CH ₃ OCHO	88851.6	7 _{1,6} -6 _{1,5} A	1.0 (0.4)	67.7 (2.6)	17.1 (5.9)	56.8 (14.0)	
H ¹⁵ NC	88865.7	1-0	1.7 (0.2)	[40, 80]	
HCO ⁺	89188.5	1-0	34.6 (0.2)	[40, 80]	
			24.6 (0.2)	[80, 110]	
CH ₃ OCHO ^c	89316.6	8 _{1,8} -7 _{1,7} A+E	1.4 (0.2)	66.6 (0.6)	25.7 (1.6)	101.4 (5.1)	bl
¹³ CH ₃ CN	89331.3	5 _K -4 _K K=0, 1	2.0 (0.2)	69.7 (1.0)	25.6 (2.5)	74.9 (4.9)	hf, bl
HCCNC	89419.3	9-8	0.7 (0.3)	70.1 (3.1)	21.5 (8.1)	28.8 (6.9)	hf
HOC ⁺	89487.4	1-0	1.1 (0.1)	68.0 (0.8)	19.4 (2.0)	51.8 (4.3)	
HCOOH	89579.1	4 _{0,4} -3 _{0,3}	2.4 (0.2)	66.5 ^a (0.8)	20.0 (1.9)	91.0 ^a (6.6)	
HCOOH	89861.4	4 _{2,3} -3 _{2,2}	1.0 (0.3)	60.3 (2.7)	25.4 (7.1)	36.8 (4.6)	
C ₂ H ₅ OH	90117.6	4 _{1,4} -3 _{0,3}	6.7 (0.3)	65.0 (0.3)	21.6 (0.8)	290.8 (7.9)	
CH ₃ OCHO	90145.6	7 _{2,5} -6 _{2,4} E	1.1 (0.4)	64.7 (2.5)	16.9 (6.3)	58.3 (9.7)	
CH ₃ OCHO	90156.4	7 _{2,5} -6 _{2,4} A	1.1 (0.3)	66.0 (1.5)	18.1 (3.9)	57.4 (7.5)	
HCOOH	90164.6	4 _{2,2} -3 _{2,1}	1.5 (0.5)	65.8 (1.9)	17.3 (4.6)	81.0 (14.6)	cl
CH ₃ COOH	90203.3	8 _{*,8} -7 _{*,7} E	≤0.3	≤33	
CH ₃ OCHO ^c	90229.6	8 _{0,8} -7 _{0,7} A+E	1.1 (0.3)	69.9 (0.9)	18.8 (2.1)	88.9 (9.0)	bl
C ₂ H ₅ CN	90453.2	10 _{2,8} -9 _{2,7}	1.6 (0.3)	70.2 (1.4)	25.2 (3.4)	58.6 (5.3)	
HC ₅ N	90526.2	34-33	2.0 (0.2)	67.1 (0.9)	23.6 (2.2)	78.3 (6.2)	
HC ¹³ CCN	90593.0	10 _K -9 _K , K=9-8, 10-9, 11-10	5.5 (0.5)	65.7 (1.1)	25.2 (2.1)	203.6 (9.2)	hf
HCC ¹³ CN	90601.7	10 _K -9 _K , K=9-8, 10-9, 11-10	3.8 (0.4)	68.8 (0.9)	22.6 (1.9)	158.3 (6.6)	hf
HNC	90663.5	1-0	39.4 (0.3)	[40, 80]	
			17.1 (0.3)	[80, 110]	
SiS	90771.5	5-4	3.6 (1.0)	69.5 ^a (3.7)	25.2 (6.6)	136.1 (12.3)	
(CH ₃) ₂ O ^b	90938.0	6 _{0,6} -5 _{1,5}	4.2 (0.4)	66.9 (0.6)	21.9 (1.4)	179.1 (11.1)	
HC ₃ N	90979.0	10-9	64.3 (1.8)	67.4 (0.2)	23.6 (0.5)	2557.7 (46.4)	
C ₂ H ₅ CN	91549.1	10 _{1,9} -9 _{1,8}	2.2 (0.5)	64.1 (2.1)	27.1 (4.5)	75.4 (7.4)	
Unidentified	91750.0		1.6 (0.2)	70.3 (0.8)	18.6 (2.0)	78.5 (7.8)	
Unidentified	91848.0		3.7 (0.3)	67.4 (0.7)	21.4 (1.6)	160.3 (8.3)	

Table 1 – *continued*

Molecule	Frequency (MHz)	Transition	Area (σ) (K km s ⁻¹)	V _{LSR} (σ) (km s ⁻¹)	$\Delta v_{1/2}$ (σ) (km s ⁻¹)	T [*] A (σ) (mK)	Notes
CH ₃ ¹³ CN	91941.5	5 _K -4 _K , K=0, 1	1.7 (0.4)	67.7 (1.6)	24.8 (3.9)	64.9 (8.5)	hf, m
CH ₃ CN, v8=0,1	91959.2	5 ₄ -4 ₄	1.9 (0.6)	71.7 (1.7)	17.4 (3.9)	102.2 (19.2)	hf
CH ₃ CN, v8=0,1	91971.3	5 ₃ -4 ₃	6.4 (0.8)	70.4 (0.8)	21.8 (2.0)	275.2 (19.4)	hf
CH ₃ CN, v8=0,1	91980.0	5 ₂ -4 ₂	6.5 (1.3)	69.3 (1.4)	16.6 ^a (2.7)	370.0 ^a (44.0)	hf
CH ₃ CN, v8=0,1	91987.0	5 _K -4 _K , K=0, 1	19.1 (0.8)	73.6 (0.4)	24.8 (0.9)	722.4 (15.8)	hf, m
C ₂ H ₃ CN	92426.2	10 _{1,10} -9 _{1,9}	1.2 (0.2)	67.9 (0.8)	18.3 (1.8)	62.0 (4.6)	
¹³ CS	92494.3	2-1	4.7 (0.5)	[45,80]	
Unidentified	92724.8		2.5 (0.3)	66.3 (1.0)	29.0 (2.3)	81.0 (6.0)	
NH ₂ CHO	105464.2	5 _{0,5} -4 _{0,4}	7.7 (0.3)	64.6 (0.3)	24.1 (0.8)	299.6 (8.9)	hf
HNCS, a-type	105558.0	9 _{0,9} -8 _{0,8}	1.6 (0.2)	64.4 (0.8)	21.6 (1.8)	68.3 (4.6)	
¹³ C ¹⁵ N	105747.7	1 _{2,1} -0 _{1,0}	1.9 (0.2)	67.9 (1.0)	23.7 (2.3)	73.5 (6.2)	hf, cl
CH ₂ NH	105793.9	4 _{0,4} -3 _{1,3}	2.4 (0.4)	71.5 ^a (1.0)	14.4 (1.7)	157.0 (18.8)	hf, bl
H ¹³ CCCN	105799.0	12 _K -11 _K , K=12-11, 13-12, 11-10	2.7 (0.4)	70.5 (1.0)	14.4 (1.9)	173.2 (7.7)	hf, bl
NH ₂ CHO	105972.6	5 _{2,4} -4 _{2,3}	2.5 (0.2)	67 (0.6)	21.9 (1.4)	105.4 (6.0)	hf
Unidentified	106302.5		2.8 (0.8)	68.5 (3.0)	21.5 (5.6)	124.1 (9.1)	
Unidentified	106311.8		4.9 (0.5)	70.0 (0.8)	21.5 (1.9)	214.0 (12.0)	
CCS	106347.7	8 ₉ -7 ₈	2.2 (0.1)	66.9 (0.4)	19.6 ^a (0.9)	104.8 (4.6)	
HC ₅ N	106499.4	40-39	1.3 (0.4)	64.5 ^a (3.0)	21.4 (5.3)	56.5 (9.0)	
NH ₂ CHO	106541.7	5 _{2,3} -4 _{2,2}	2.2 (0.2)	68.6 (0.8)	21.4 (1.8)	95.6 (6.6)	hf
C ₂ H ₃ CN	106641.3	11 _{1,10} -10 _{1,9}	1.0 (0.2)	74.2 (0.9)	16.7 (2.2)	56.0 (6.9)	
(CH ₃) ₂ O ^b	106777.3	9 _{1,8} -8 _{2,7}	0.9 (0.3)	72.2 (1.9)	14.3 (4.3)	60.0 (11.2)	
OC ³⁴ S	106787.3	9-8	1.6 (0.2)	67.5 ^a (0.9)	21.4 (2.3)	69.3 (4.9)	
HOCO ⁺	106913.5	5 _{0,5} -4 _{0,4}	13.6 (0.4)	68.0 (0.2)	21.1 (0.5)	606.0 (11.8)	
CH ₃ OH	107013.8	3 _{1,3} -4 _{0,4} A+	-2.7 (...)	66.1 (3.1)	40.0 (7.0)	-64.1 (...)	al
C ₂ H ₅ CN	107043.5	12 _{2,11} -11 _{2,10}	1.8 (0.3)	68.7 (1.3)	21.3 (3.2)	77.8 (9.1)	
Unidentified	107100.0		0.9 (0.2)	68.5 (1.3)	18.6 (3.1)	47.2 (6.5)	
Unidentified	107134.6		3.2 (0.2)	70.6 (0.5)	21.4 (1.1)	139.6 (6.2)	
¹³ CH ₃ CN	107178.5	6 ₃ -5 ₃	0.5 (0.2)	72.4 (1.8)	16.4 (4.2)	28.7 (7.2)	hf
¹³ CH ₃ CN	107196.5	6 _K -5 _K , K=0, 1	1.5 (0.2)	74.6 (1.0)	21.3 (2.23)	66.1 (5.68)	hf, bl
HCOOH	108126.7	5 _{1,5} -4 _{1,4}	2.2 (0.3)	67.5 ^a (1.0)	21.1 ^a (2.5)	97.8 (5.2)	
¹³ CN	108636.9	N=1-0, F1=0, F2=1-0, F=1-1	2.5 (0.6)	57.6 (4.1)	35.0 (7.3)	67.2 (6.3)	hf
¹³ CN	108651.2	N=1-0, F1=0, F2=1-0, F=2-1	2.0 (0.4)	56.8 (2.3)	32.6 (4.8)	56.7 (5.6)	hf
HC ¹³ CCN	108710.5	12 _K -11 _K , K=12-11, 13-12, 11-10	2.3 (0.4)	69.0 (1.9)	25.4 (3.8)	86.1 (6.5)	hf
HCC ¹³ CN	108721.0	12 _K -11 _K , K=12-11, 13-12, 11-10	1.6 (0.3)	68.7 (1.7)	22.0 (3.8)	68.7 (6.4)	hf
¹³ CN	108780.2	N=1-0, F1=1, F2=2-1, F=3-2	1.6 (0.2)	69.4 (0.9)	21.0 (2.1)	71.8 (5.9)	hf
¹³ CN	108786.9	N=1-0, F1=1, F2=2-1, F=1-0	0.7 (0.2)	69.8 (1.0)	13.3 (2.7)	51.2 (6.1)	hf ^a
¹³ CN	108796.4	N=1-0, F1=1, F2=2-1, F=2-2	0.9 (0.2)	71.3 (1.0)	17.8 (2.4)	48.9 (5.9)	hf, cd
CH ₃ OH	108893.9	0 _{0,0} -1 _{-1,1} E	12.1 (0.3)	[40,80]	
			2.4 (0.3)	[80,110]	
O ¹³ CS	109110.8	9-8	0.6 (0.2)	66.4 (1.7)	17.1 (3.9)	32.4 (7.8)	
HC ₃ N	109173.6	12-11	47.3 (1.2)	66.9 (0.2)	23.0 (0.4)	1932.8 (31.5)	
SO	109252.2	3 ₂ -2 ₁	8.2 (0.3)	67.6 (0.2)	20.3 (0.5)	380.4 (7.9)	
OCS	109463.0	9-8	19.5 (0.5)	65.8 (0.2)	22.4 (0.4)	819.0 (13.4)	
HNCO	109496.0	5 _{1,5} -4 _{1,4}	2.8 (0.4)	64.3 (1.0)	20.7 (2.4)	127.1 (12.5)	hf
C ₂ H ₅ CN	109650.2	12 _{1,11} -11 _{1,10}	2.0 (0.3)	64.6 (1.4)	27.9 (3.3)	67.3 (7.7)	
NH ₂ CHO	109753.5	5 _{1,4} -4 _{1,3}	5.0 (0.4)	66.9 (0.5)	21.5 (1.2)	220.2 (10.4)	hf
C ¹⁸ O	109782.1	1-0	23.4 (0.9)	66.8 (0.3)	25.7 (0.8)	855.2 (21.5)	
HNCO	109905.7	5 _{0,5} -4 _{0,4}	111.9 (2.7)	67.6 (0.2)	23.8 (0.4)	4420.4 (68.9)	hf
¹³ CO	110201.3	1-0	148.6 (5.5)	67.5 ^a (0.3)	27.6 (0.9)	5052.1 (95.0)	
HNCO	110298.0	5 _{1,4} -4 _{1,3}	3.5 (0.6)	63.1 (1.3)	20.7 (3.1)	157.0 ^a (13.9)	hf
CH ₃ ¹³ CN	110328.8	6 _K -5 _K , K=0, 1	2.0 (0.3)	69.7 (0.8)	20.7 (2.0)	89.3 (7.8)	hf, m, cd
CH ₃ CN, v8=0,1	110349.7	6 ₄ -5 ₄	1.4 (0.6)	70.0 (2.2)	15.6 (5.3)	82.0 (23.0)	hf
CH ₃ CN, v8=0,1	110364.4	6 ₃ -5 ₃	7.5 (0.8)	68.5 (0.7)	20.7 (1.8)	338.1 (18.4)	hf
CH ₃ CN, v8=0,1	110374.9	6 ₂ -5 ₂	8.6 (2.6)	70.5 ^a (1.8)	20.7 (6.1)	390.0 ^a (26.9)	hf
CH ₃ CN, v8=0,1	110383.4	6 _K -5 _K , K=0, 1	25.1 (0.9)	74.2 (0.3)	27.6 (0.8)	853.4 (16.4)	hf, m
CH ₃ OCHO ^c	110790.5	10 _{1,10} -9 _{1,9} A+E	0.8 (0.2)	70.7 (0.7)	20.6 (1.8)	71.7 (5.4)	bl
CH ₃ OCHO ^c	111682.1	9 _{1,8} -8 _{1,7} A+E	1.4 (0.6)	76.6 (2.1)	27.3 (5.0)	96.0 ^a (7.1)	bl
HCOOH	111746.7	5 _{0,5} -4 _{0,4}	2.9 (0.5)	70.4 ^a (1.6)	20.4 ^a (3.3)	134.5 (8.4)	
(CH ₃) ₂ O ^b	111783.0	7 _{0,7} -6 _{1,6}	3.5 (0.4)	65.3 (0.8)	20.4 (1.9)	159.4 (11.5)	
CH ₃ CHO	112248.7	6 _{1,6} -5 _{1,5} A	3.8 (0.6)	61.8 (0.8)	31.7 (1.8)	226.9 (12.2)	bl
CH ₃ CHO	112254.5	6 _{-1,6} -5 _{-1,5} E	3.8 (0.5)	77.3 (0.7)	31.7 (1.6)	0.2 (10.4)	bl
C ¹⁷ O	112358.9	1-0	5.0 (0.5)	65.7 (0.7)	23.6 (1.7)	200.7 (11.8)	
Unidentified	112464.0		1.9 (1.0)	68.6 (4.0)	26.2 (8.0)	68.8 (20.0)	
C ₂ H ₅ OH	112807.1	2 _{2,1} -1 _{1,0}	4.2 (0.4)	67.2 (0.9)	30.3 (2.4)	130.9 (6.2)	
CN	113123.3	N=1-0, J=1/2-1/2, F=1/2-1/2	3.8 (0.4)	70.5 ^a (0.5)	13.5 (1.1)	264.0 ^a (14.6)	hf ^a , ot, cd
CN	113144.1	N=1-0, J=1/2-1/2, F=1/2-3/2	0.8 (0.2)	[49.5, 79.5]	hf ^a
CN	113170.5	N=1-0, J=1/2-1/2, F=3/2-1/2	2.5 (0.2)	[49.5, 79.5]	hf ^a
CN	113191.3	N=1-0, J=1/2-1/2, F=3/2-3/2	1.9 (0.2)	[49.5, 79.5]	hf ^a
CN	113490.9	N=1-0, J=3/2-1/2, F=5/2-3/2	7.0 (0.2)	[49.5, 79.5]	hf
CN	113508.9	N=1-0, J=3/2-1/2, F=3/2-3/2	2.3 (0.2)	[49.5, 79.5]	hf ^a

Notes: (bl) blended line; (m) multitransition line (frequency refers to the main component of the group); (hf) hyperfine structure (frequency refers to the main component of the group); (hf^a) hyperfine component, it is possible to resolve this hyperfine component since its frequency is sufficiently far from the frequencies of the other hyperfine components; (ot) transition less affected by opacity; (cl) this line is contaminated by the emission from an unknown molecular species; (al) absorption line; (cd) this transition is used to derive the column density (although several transitions of this molecule are detected, there is an insufficient dynamical range in E_u to derive the column density by using a RD).

^a Parameter fixed in the Gaussian fit.

^b Substates EE, AA, EA, AE blended, we show just the most intense transition.

^c Frequency refers to species A.

Table 2. Line parameters for *LOS*–0.11.

Molecule	Frequency (MHz)	Transition	Area (σ) (K km s ⁻¹)	V _{LSR} (σ) (km s ⁻¹)	$\Delta v_{1/2}$ (σ) (km s ⁻¹)	T _a [*] (σ) (mK)	Notes
C ₂ H ₃ CN	77633.8	8 _{1,7} -7 _{1,6}	1.8 (0.4)	21.9 (1.2)	19.6 (2.9)	88.0 (12.0)	
CH ₃ CHO	79099.3	4 _{1,3} -3 _{1,2} E	4.8 (0.5)	20.3 (0.7)	20.2 (1.6)	222.1 (15.6)	
CH ₃ CHO	79150.2	4 _{1,3} -3 _{1,2} A	4.5 (0.8)	17.5 (1.2)	19.2 (2.7)	220.0 ^a (23.9)	
H ¹³ CCCN	79350.4	9 _K -8 _K , K=8-7, 9-8, 10-9	2.7 (0.5)	16.7 (1.1)	19.2 (2.8)	131.0 ^a (11.7)	hf
NH ₂ CN	79449.7	4 _{1,4} -3 _{1,3}	5.9 (0.4)	20.1 (0.4)	19.2 (1.0)	290.0 ^a (11.7)	
C ₂ H ₅ CN	79677.5	9 _{0,9} -8 _{0,8}	1.8 (0.3)	16.2 (1.2)	19.1 (2.9)	87.0 ^a (9.4)	
HC ₅ N	79876.9	30-29	2.4 (0.3)	18.2 (0.8)	19.6 (1.8)	115.8 (9.4)	
NH ₂ CN	79963.2	4 _{2,3} -3 _{2,2}	1.3 (0.3)	17.6 (1.5)	19.0 (3.6)	65.0 ^a (9.3)	m
NH ₂ CN	79979.5	4 _{0,4} -3 _{0,3}	2.5 (0.4)	21.2 (1.0)	19.0 (2.4)	124.0 ^a (13.1)	
CH ₂ CO	80076.7	4 _{1,4} -3 _{1,3}	2.2 (0.2)	20.7 (0.5)	17.2 (1.1)	119.6 (6.2)	
Unidentified	80282.8		0.9 (0.2)	18.5 (1.0)	15.8 (2.3)	51.3 (6.2)	
Unidentified	80373.6		1.5 (0.4)	20.0 (2.5)	29.1 (5.5)	48.2 (8.3)	
C ₂ H ₅ CN	80404.9	9 _{2,8} -8 _{2,7}	1.0 (0.3)	17.2 (2.3)	24.7 ^a (5.5)	39.2 (8.1)	
H ₂ C ₂ N	80480.9	4 _{0,4} -3 _{0,3} , J=9/2-7/2	2.1 (0.4)	17.6 (1.2)	19.7 (2.9)	100.3 (8.1)	hf ^a , cd
H ₂ C ₂ N	80489.9	4 _{0,4} -3 _{0,3} , J=7/2-5/2	2.2 (0.4)	20.6 (1.0)	18.9 (2.5)	105.3 (8.6)	hf ^a
NH ₂ CN	80504.6	4 _{1,3} -3 _{1,2}	5.1 (0.6)	21.2 (0.6)	18.9 (1.5)	260.9 (17.7)	
(CH ₃) ₂ O ^b	80538.5	5 _{2,3} -5 _{1,4}	1.9 (0.4)	20.2 (1.9)	28.4 (4.4)	61.8 (8.0)	
CH ₂ CO	80832.1	4 _{0,4} -3 _{0,3}	1.3 (0.3)	21.2 (1.6)	18.8 (3.8)	53.0 ^a (7.1)	
CH ₃ OH	80993.2	7 _{2,6} -8 _{1,7} A-	≤0.3	≤33	cd
HNO	81477.4	1 _{0,1} -0 _{0,0}	1.2 (0.2)	17.2 ^a (1.2)	20.6 (2.7)	53.4 (6.4)	hf
CCS	81505.1	7 ₆ -6 ₅	3.4 (0.5)	20.8 (1.0)	19.9 (2.3)	159.2 (13.4)	
HC ¹³ CCN	81534.1	9 _K -8 _K , K=8-7, 9-8, 10-9	1.8 (0.2)	19.0 (0.6)	17.5 (1.5)	96.3 (4.8)	hf
HCC ¹³ CN	81541.9	9 _K -8 _K , K=8-7, 9-8, 10-9	2.1 (0.2)	18.4 (0.5)	18.4 (1.2)	108.5 (5.0)	hf
CH ₂ CO	81586.2	4 _{1,3} -3 _{1,2}	2.4 (0.2)	15.9 (0.4)	18.7 (0.9)	120.0 ^a (4.52)	
NH ₂ CHO	81693.5	4 _{1,4} -3 _{1,3}	3.0 (0.3)	11.0 (0.7)	18.1 (1.7)	157.3 (10.0)	hf
HC ₃ N	81881.4	9-8	50.0 (0.6)	17.4 (0.1)	18.6 (0.2)	2527.7 (19.7)	
c-C ₃ H ₂	82093.5	2 _{0,2} -1 _{1,1}	4.7 (0.3)	19.9 (0.3)	17.8 (0.8)	246.3 (9.1)	
HNCS, a-type	82101.8	7 _{0,7} -6 _{0,6}	0.9 (0.3)	21.2 ^a (2.0)	18.5 (4.7)	45.0 ^a (8.3)	
Unidentified	82198.8		0.6 (0.2)	17.2 (1.8)	18.5 (4.3)	30.2 (5.5)	
C ₂ H ₅ CN	82458.5	9 _{1,8} -8 _{1,7}	1.4 (0.4)	23.9 (1.8)	18.5 (4.2)	69.0 ^a (10.3)	
HCOCH ₂ OH	82470.6	8 _{0,8} -7 _{1,7}	≤0.7	≤60	
HC ₅ N	82539.2	31-30	1.9 (0.4)	18.0 (0.6)	21.0 (1.6)	76.3 (3.7)	
NH ₂ CHO	82549.5	1 _{1,1} -0 _{0,0}	0.4 (0.1)	17.2 (1.4)	18.4 (3.4)	25.1 (4.0)	hf, cl
c-C ₃ H ₂	82966.2	3 _{1,2} -3 _{0,3}	2.1 (0.1)	18.1 (0.4)	18.4 (1.0)	108.3 (4.8)	
OC ³⁴ S	83057.9	7-6	≤0.3	≤39	
HNC ¹⁸ O	83191.5	4 _{0,4} -3 _{0,3}	≤0.1	≤30	hf
C ₂ H ₃ CN	83207.5	9 _{1,9} -8 _{1,8}	0.7 (0.2)	18.2 ^a (1.2)	17.2 (2.8)	37.7 (5.2)	
SO ₂	83688.0	8 _{1,7} -8 _{0,8}	1.0 (0.2)	18.6 (1.0)	17.5 (2.4)	55.6 (6.5)	
Unidentified	83900.3		2.0 (0.2)	14.6 (0.5)	16.7 (1.1)	111.0 (6.2)	
¹³ CCH	84153.3	N=1-0, F ₁ =1-0, F=3/2-1/2	1.0 (0.3)	27.9 (2.3)	27.1 (5.4)	34.1 (5.9)	hf
CH ₃ CHO	84219.7	2 _{1,2} -1 _{0,1} A	0.9 (0.6)	22.2 ^a (3.4)	18.1 (...)	47.0 ^a (6.1)	
CH ₃ OH	84521.1	5 _{-1,5} -4 _{0,4} E	50.0 (2.0)	19.0 (0.2)	15.0 (0.5)	3140.3 (80.2)	
NH ₂ CHO	84542.4	4 _{0,4} -3 _{0,3}	3.9 (0.3)	19.3 (0.4)	16.4 (1.0)	223.7 (8.2)	hf
³⁰ SiO	84745.9	2-1	1.8 (0.2)	19.7 (0.5)	17.8 (1.1)	95.0 (5.2)	
NH ₂ CHO	84807.9	4 _{2,3} -3 _{2,2}	0.5 (0.1)	21.2 (0.6)	10.4 (1.3)	41.2 (4.7)	hf
O ¹³ CS	84865.1	7-6	≤0.3	≤36	
C ₂ H ₃ CN	84946.0	9 _{0,9} -8 _{0,8}	1.0 (0.1)	18.8 (0.6)	15.4 (1.3)	60.3 (4.3)	
¹³ CH ₃ OH	84970.2	8 _{0,8} -7 _{1,7} A+	≤0.2	≤24	
NH ₂ CHO	85093.3	4 _{2,2} -3 _{2,1}	1.1 (0.3)	21.8 (1.5)	20.0 (3.5)	53.1 (7.6)	hf
OCS	85139.1	7-6	10.3 (0.4)	17.9 (0.2)	18.2 (0.6)	534.9 (12.9)	
HC ¹⁸ O ⁺	85162.1	1-0	1.2 (0.2)	23.4 (1.2)	20.9 (2.8)	55.6 (6.4)	
HC ₅ N	85201.6	32-31	2.0 (0.4)	22.8 (1.2)	17.9 (2.9)	104.1 (13.2)	
C ¹³ CH	85229.3	N=1-0, F ₁ =2-1 F=5/2-3/2	≤0.7	≤81	hf
C ₂ H ₅ OH	85265.5	6 _{0,6} -5 _{1,5}	3.3 (0.2)	21.2 (0.3)	18.7 ^a (0.7)	163.8 (5.7)	cl
H ¹⁵ NCO	85292.1	4 _{0,4} -3 _{0,3}	≤0.3	≤27	
c-C ₃ H ₂	85338.8	2 _{1,2} -1 _{0,1}	0.8 (0.2)	19.2 ^a (2.1)	18.0 (5.0)	40.0 ^a (6.0)	
HCS ⁺	85347.9	2-1	2.5 (0.6)	21.8 (1.7)	17.8 (4.2)	133.4 (13.3)	
CH ₃ ¹³ CCH	85421.8	5 _K -4 _K , K=0, 1	≤0.3	≤39	m
CH ₃ CCH	85442.5	5 ₃ -4 ₃	0.8 (0.1)	21.2 ^a (7.4)	17.8 (...)	42.1 (...)	
CH ₃ CCH	85450.7	5 ₂ -4 ₂	0.9 (0.2)	22.2 ^a (1.1)	17.8 (2.9)	47.8 (5.1)	bl
CH ₃ CCH	85457.2	5 _K -4 _K , K=0, 1	3.7 (0.3)	18.5 (0.5)	17.8 (1.1)	196.7 (9.5)	m
HOCO ⁺	85531.5	4 _{0,4} -3 _{0,3}	6.7 (0.2)	18.5 (0.2)	18.4 (0.5)	341.1 (8.3)	
²⁹ SiO	85759.0	2-1	4.1 (0.6)	21.8 (1.0)	21.8 (2.4)	177.0 ^a (16.2)	
HC ¹⁵ N	86054.9	1-0	3.6 (0.4)	[-0.8 47.2]	
SO	86093.9	2 ₂ -1 ₁	3.3 (0.9)	19.9 (1.7)	18.9 (4.0)	162.0 ^a (29.0)	
H ¹³ CN	86340.1	1-0, F=1-1, 2-1, 0-1	27.1 (0.3)	[-0.8 47.2]	hf
HCO	86708.3	1 _{0,1} -0 _{0,0} , J=3/2-1/2, F=1-0	≤0.8	≤96	hf ^a
H ¹³ CO ⁺	86754.2	1-0	10.1 (0.3)	[0.2 36.2]	
SiO	86846.9	2-1	33.2 (0.9)	18.2 ^a (0.2)	20.3 (0.4)	1537.8 (27.4)	
HN ¹³ C	87090.8	1-0	14.4 (0.6)	16.8 (0.3)	19.3 (0.6)	697.2 (18.2)	
CCH	87284.1	N=1-0, J=3/2-1/2, F=1-1	3.9 (0.4)	19.8 (0.6)	21.3 (1.5)	173.8 (11.6)	hf ^a , cd
CCH	87316.9	N=1-0, J=3/2-1/2, F=2-1	19.3 (0.7)	18.5 (0.2)	18.6 (0.5)	971.7 (22.3)	hf ^a
CCH	87328.6	N=1-0, J=3/2-1/2, F=1-0	7.0 (0.6)	18.3 (0.5)	15.7 (1.1)	419.0 (24.3)	hf ^a
CCH	87402.0	N=1-0, J=1/2-1/2, F=1-1	16.4 (0.7)	15.6 (0.4)	26.1 (0.9)	590.0 ^a (14.4)	hf ^a , bl
CCH	87407.1	N=1-0, J=1/2-1/2, F=0-1	4.0 (1.9)	20.8 (5.8)	22.5 (7.5)	164.8 (58.9)	hf ^a , bl
CCH	87446.5	N=1-0, J=1/2-1/2, F=1-0	2.9 (0.6)	18.1 (1.1)	17.5 (2.5)	157.4 (19.1)	hf ^a

Table 2 – *continued*

Molecule	Frequency (MHz)	Transition	Area (σ) (K km s ⁻¹)	V _{LSR} (σ) (km s ⁻¹)	$\Delta v_{1/2}$ (σ) (km s ⁻¹)	T _a [*] (σ) (mK)	Notes
HNCO	87597.3	4 _{1,4} -3 _{1,3}	1.4 (0.5)	19.2 ^a (2.1)	17.4 (5.1)	75.0 ^a (13.4)	hf
NH ₂ CHO	87848.9	4 _{1,3} -3 _{1,2}	4.1 (0.5)	17.9 (0.7)	18.4 (1.8)	211.3 (17.5)	hf
HC ₅ N	87863.9	33-32	2.3 (0.4)	20.0 (0.9)	17.3 (2.2)	126.6 (12.5)	
HNCO	87925.2	4 _{0,4} -3 _{0,3}	62.4 (1.1)	17.7 (0.1)	17.5 (0.2)	3358.4 (39.0)	hf
H ¹³ CCCN	88166.8	10 _K -9 _K , K=10-9, 11-10, 9-8	2.1 (0.4)	23.6 (1.0)	17.3 (2.4)	113.3 (11.0)	hf
HCN	88631.8	1-0, F=0-1, 1-1, 2-1	123.8 (0.2)	[-0.8 47.2]	hf
CH ₃ OCHO	88843.2	7 _{1,6} -6 _{1,5} E	1.2 (0.4)	17.7 (2.1)	17.1 (5.1)	65.0 ^a (11.3)	
H ¹⁵ NC	88865.7	1-0	1.1 (0.2)	21.5 (1.3)	20.2 (3.2)	52.1 (7.8)	
HCO ⁺	89188.5	1-0	74.2 (0.2)	[0.2 36.2]	
HCCNC	89419.3	9-8	≤0.3	≤39	hf
HOC ⁺	89487.4	1-0	≤0.3	≤39	
HCOOH	89579.1	4 _{0,4} -3 _{0,3}	1.2 (0.2)	18.6 (0.9)	18.4 (2.1)	60.6 (6.2)	cd
HCOOH	89861.4	4 _{2,3} -3 _{2,2}	1.7 (0.3)	20.3 (2.3)	30.0 (4.1)	46.1 (6.7)	
C ₂ H ₅ OH	90117.6	4 _{1,4} -3 _{0,3}	2.5 (0.2)	18.6 (0.5)	16.9 (1.1)	138.4 (7.8)	cd
CH ₃ COOH	90203.3	8 _{*,8} -7 _{*,7} E	≤0.3	≤36	
HC ₅ N	90526.2	34-33	2.0 (0.2)	19.1 (0.7)	18.4 (1.6)	102.0 (8.1)	
HC ¹³ CCN	90593.0	10 _K -9 _K , K=9-8, 10-9, 11-10	1.9 (0.2)	20.5 (0.6)	16.8 (1.5)	103.3 (7.6)	hf
HCC ¹³ CN	90601.7	10 _K -9 _K , K=9-8, 10-9, 11-10	0.8 (0.2)	18.7 (1.3)	15.1 (3.2)	52.2 (8.6)	hf
HNC	90663.5	1-0	101.3 (3.6)	19.1 (0.3)	25.7 (0.7)	3709.2 (85.1)	
SiS	90771.5	5-4	1.4 (0.3)	21.2 ^a (1.1)	16.8 (2.6)	78.5 (11.0)	
(CH ₃) ₂ O ^b	90938.0	6 _{0,6} -5 _{1,5}	2.5 (0.5)	17.8 (2.0)	27.7 (4.7)	84.0 ^a (8.8)	
HC ₃ N	90979.0	10-9	47.4 (0.8)	18.3 (0.1)	18.2 (0.2)	2441.8 (26.1)	
C ₂ H ₅ CN	91549.1	10 _{1,9} -9 _{1,8}	1.1 (0.5)	20.3 (2.3)	16.6 (6.1)	64.0 ^a (13.1)	
Unidentified	91848.0		3.1 (0.4)	23.0 (1.3)	24.9 (2.9)	115.9 (8.0)	
CH ₃ CN, v8=0,1	91959.2	5 ₄ -4 ₄	1.0 (0.3)	21.6 (1.3)	12.3 (3.2)	75.9 (16.6)	hf
CH ₃ CN, v8=0,1	91971.3	5 ₃ -4 ₃	4.5 (0.4)	20.8 (0.4)	15.2 (1.0)	277.2 (14.6)	hf
CH ₃ CN, v8=0,1	91980.0	5 ₂ -4 ₂	4.6 (0.5)	20.2 ^a (0.5)	16.6 (1.2)	259.0 ^a (16.4)	hf
CH ₃ CN, v8=0,1	91987.0	5 _K -4 _K , K=0, 1	17.9 (0.5)	17.2 ^a (0.2)	21.1 (0.5)	793.5 (13.0)	hf, m
¹³ CS	92494.3	2-1	5.7 (0.2)	18.7 (0.2)	21.3 (0.6)	251.8 (5.6)	
Unidentified	92724.8		0.8 (0.2)	17.2 (1.4)	16.4 (3.3)	46.5 (7.7)	
NH ₂ CHO	105464.2	5 _{0,5} -4 _{0,4}	2.0 (0.4)	22.5 (0.8)	14.4 (2.0)	127.3 (14.5)	hf
CH ₂ NH	105793.9	4 _{0,4} -3 _{1,3}	1.9 (0.6)	17.8 (2.6)	20.5 (5.9)	90.2 (12.7)	hf, bl
H ¹³ CCCN	105799.0	12 _K -11 _K , K=12-11, 13-12, 11-10	1.0 (0.5)	13.2 ^a (3.3)	14.4 (6.7)	66.0 ^a (18.8)	hf, bl
Unidentified	106273.2		6.4 (0.6)	17.4 (0.7)	24.3 (1.6)	247.0 (14.2)	
CCS	106347.7	8 ₉ -7 ₈	1.9 (0.5)	20.1 (1.6)	18.7 (4.1)	93.5 (12.5)	
HOCO ⁺	106913.5	5 _{0,5} -4 _{0,4}	4.7 (0.4)	20.7 (0.4)	15.3 (1.0)	290.4 (17.5)	
CH ₃ OH	107013.8	3 _{1,3} -4 _{0,4} A+	-2.7 (...)	19.4 (2.3)	33.8 (5.0)	-76.0 (...)	al
¹³ CH ₃ CN	107196.5	6 _K -5 _K , K=0, 1	≤0.5	≤69	hf, m
¹³ CN	108636.9	N=1-0, F1=0, F2=1-0, F=1-1	2.6 (0.6)	21.0 ^a (4.0)	35.0 (8.0)	69.0 ^a (5.8)	hf, cd
¹³ CN	108651.2	N=1-0, F1=0, F2=1-0, F=2-1	1.6 (0.4)	15.4 ^a (1.7)	21.0 (4.0)	73.0 (10.0)	hf
HC ¹³ CCN	108710.5	12 _K -11 _K , K=12-11, 13-12, 11-10	1.5 (0.3)	19.1 (1.5)	18.2 (3.5)	77.9 (9.4)	hf
HCC ¹³ CN	108721.0	12 _K -11 _K , K=12-11, 13-12, 11-10	1.3 (0.3)	19.1 (1.2)	14.0 ^a (2.8)	86.0 ^a (10.5)	hf
¹³ CN	108780.2	N=1-0, F1=1, F2=2-1, F=3-2	2.1 (0.4)	14.7 (1.0)	20.9 (2.3)	98.5 (11.7)	hf
¹³ CN	108786.9	N=1-0, F1=1, F2=2-1, F=1-0	0.7 (0.3)	22.2 ^a (0.8)	7.0 (2.0)	98.0 (20.5)	hf ^a
CH ₃ OH	108893.9	0 _{0,0} -1 _{-1,1} E	10.3 (0.3)	17.5 (0.2)	20.6 (0.5)	471.5 (10.0)	
HC ₃ N	109173.6	12-11	24.3 (0.5)	17.5 (0.1)	16.5 (0.3)	1389.9 (19.0)	
SO	109252.2	3 ₂ -2 ₁	3.7 (1.2)	21.2 (2.5)	17.7 (4.9)	196.0 ^a (30.9)	
Unidentified	109353.8		1.9 (0.3)	20.4 (0.9)	20.1 (2.2)	83.3 (7.2)	
OCS	109463.0	9-8	8.9 (0.4)	20.0 (0.3)	19.1 (0.7)	440.5 (12.9)	
HNCO	109496.0	5 _{1,5} -4 _{1,4}	0.8 (0.5)	14.2 ^a (2.7)	13.9 (7.4)	55.0 ^a (13.9)	hf
NH ₂ CHO	109753.5	5 _{1,4} -4 _{1,3}	2.2 (0.6)	22.0 (1.2)	13.9 (2.8)	148.7 (26.1)	hf
C ¹⁸ O	109782.1	1-0	9.5 (0.8)	15.1 (0.6)	21.7 (1.4)	441.8 (22.7)	bl
			2.5 (0.8)	55.2 (2.1)	21.7 (5.1)	108.0 (22.6)	
HNCO	109905.7	5 _{0,5} -4 _{0,4}	58.3 (1.1)	18.2 (0.1)	18.4 (0.3)	2980.2 (36.1)	hf
¹³ CO	110201.3	1-0	83.6 (3.1)	16.0 (0.3)	21.2 (0.6)	3701.9 (87.0)	
			27.2 (3.2)	50.2 ^a (0.8)	20.7 (2.0)	1231.5 (82.9)	
CH ¹³ CN	110328.8	6 _K -5 _K , K=0, 1	≤0.7	≤87	hf, m
CH ₃ CN, v8=0,1	110349.7	6 ₄ -5 ₄	1.0 (0.5)	18.7 (2.5)	15.6 (5.9)	57.6 (21.7)	hf
CH ₃ CN, v8=0,1	110364.4	6 ₃ -5 ₃	3.8 (0.6)	19.2 (0.8)	16.9 (1.9)	212.7 (20.87)	hf
CH ₃ CN, v8=0,1	110374.9	6 ₂ -5 ₂	3.14 (0.6)	19.2 ^a (0.9)	13.8 (2.2)	214.0 ^a (21.3)	hf
CH ₃ CN, v8=0,1	110383.4	6 _K -5 _K , K=0, 1	13.1 (0.7)	16.7 (0.4)	21.3 (1.0)	576.8 (18.3)	hf, m
(CH ₃) ₂ O ^b	111783.0	7 _{0,7} -6 _{1,6}	3.0 (0.9)	19.1 (2.8)	27.2 (6.6)	103.1 (20.4)	
CH ₃ CHO	112248.7	6 _{1,6} -5 _{1,5} A	1.2 (0.6)	17.2 ^a (2.4)	13.6 (4.8)	84.0 ^a (28.1)	bl
CH ₃ CHO	112254.5	6 _{-1,6} -5 _{-1,5} E	2.0 (0.6)	21.2 ^a (1.6)	13.6 (3.7)	139.0 ^a (9.3)	bl
C ¹⁷ O	112359.2	1-0	3.9 (1.1)	15.2 ^a (3.7)	27.1 (6.3)	134.0 ^a (20.2)	bl
			2.9 (0.5)	42.9 (1.4)	20.3 (2.7)	135.8 (11.5)	
C ₂ H ₅ OH	112807.1	2 _{2,1} -1 _{1,0}	1.6 (0.4)	17.5 (1.1)	13.5 (2.5)	114.3 (14.6)	
C ₂ H ₃ CN	112840.6	12 _{0,12} -11 _{0,11}	0.7 (0.3)	19.7 (1.0)	7.5 ^a (2.4)	91.0 ^a (25.1)	
CN	113123.3	N=1-0, J=1/2-1/2, F=1/2-1/2	5.5 (0.5)	13.9 (0.6)	20.6 (1.4)	248.8 (15.2)	hf ^a , ot, cd
CN	113144.1	N=1-0, J=1/2-1/2, F=1/2-3/2	6.2 (0.5)	15.51 (0.6)	23.7 (1.5)	247.7 (14.6)	hf ^a
CN	113170.5	N=1-0, J=1/2-1/2, F=3/2-1/2	11.4 (0.2)	[-0.2, 32.2]	hf ^a

Table 2 – continued

Molecule	Frequency (MHz)	Transition	Area (σ) (K km s ⁻¹)	V _{LSR} (σ) (km s ⁻¹)	$\Delta v_{1/2}$ (σ) (km s ⁻¹)	T _a [*] (σ) (mK)	Notes
CN	113191.3	N=1-0, J=1/2-1/2, F=3/2-3/2	6.5 (0.2)	[-0.2, 32.2]	hf ^a
CN	113490.9	N=1-0, J=3/2-1/2, F=5/2-3/2	22.4 (0.4)	[-0.2, 32.2]	hf
CN	113508.9	N=1-0, J=3/2-1/2, F=3/2-3/2	7.9 (0.4)	[-0.2, 32.2]	hf ^a

Notes: (bl) blended line; (m) multitransition line (frequency refers to the main component of the group); (hf) hyperfine structure (frequency refers to the main component of the group); (hf^a) hyperfine component, it is possible to resolve this hyperfine component since its frequency is sufficiently far from the frequencies of the other hyperfine components; (ot) transition less affected by opacity; (cl) this line is contaminated by the emission from an unknown molecular species; (al) absorption line; (cd) this transition is used to derive the column density (although several transitions of this molecule are detected, there is an insufficient dynamical range in E_u to derive the column density by using a RD).

^a Parameter fixed in the Gaussian fit.

^b Substates EE, AA, EA, AE blended, we show just the most intense transition.

^c Frequency refers to species A.

4 DISCUSSION

4.1 Uniform molecular abundances and excitation conditions in the nuclei of galaxies

4.1.1 Galactic center

Early studies of the distribution of the kinetic temperature in the molecular material in the GC using both ammonia and H₂ have shown that molecular clouds are warm with a mean T_{kin} of ≈ 100 K (Hüttemeister et al. 1993; Rodríguez-Fernández et al. 2001). More recently, Requena-Torres et al. (2006) have found that the abundance of complex organic molecules is also relatively uniform in the molecular clouds in the GC. In agreement with the findings of Requena-Torres et al. (2006), we also found that the molecular clouds toward two lines of sight, $LOS+0.693$ and $LOS-0.11$, separated by more than ~ 120 pc within the Galactic Center, show a rather uniform chemistry. $\sim 80\%$ of molecular species detected in both lines of sight show similar abundances within a factor of 2, even for the most complex organic molecules like C₂H₅OH, C₂H₅CN and (CH₃)₂O.

Our (CH₃)₂O, CH₃OH, HCOOH, HNCO, ¹³CS and C¹⁸O abundances are also consistent with those derived in previous studies toward both GC sources from 2 and 3 mm line data (Requena-Torres et al. 2006; Martín et al. 2008). The “uniform” chemistry in the GC was explained for complex molecules as due to grain surface chemistry followed by the sputtering of the icy mantles by shocks. Our database allows now a detailed comparison of the excitation conditions found along the two LOS s. Fig. 7 represents the T_{rot} derived for $LOS+0.693$ versus the T_{rot} derived for $LOS-0.11$. It is remarkable that the excitation of the molecular gas is very similar for both GC sources. In fact, 86% of the molecules show the same T_{rot} within 1σ . Another two molecules (c-C₃H₂ and NH₂CHO) show T_{rot} which are consistent within 3σ . HC₃N is the only molecule that shows a significant difference in its excitation between both GC sources above a 3σ level. However, the difference in the T_{rot} by a factor of 1.4 corresponds to a change of only a factor of 1.8 in the derived H₂ densities of the molecular gas (see section 3.3.4). The similar excitation conditions and molecular complexity found in the molecular gas in the two LOS s indicate that physical processes operating in the GC are widespread, driving the chemistry and affecting the physical conditions over large scales.

It is remarkable that the complex organic molecules like CH₂CO, HC₅N, NH₂CN, CH₃CCH and CH₃CN show the

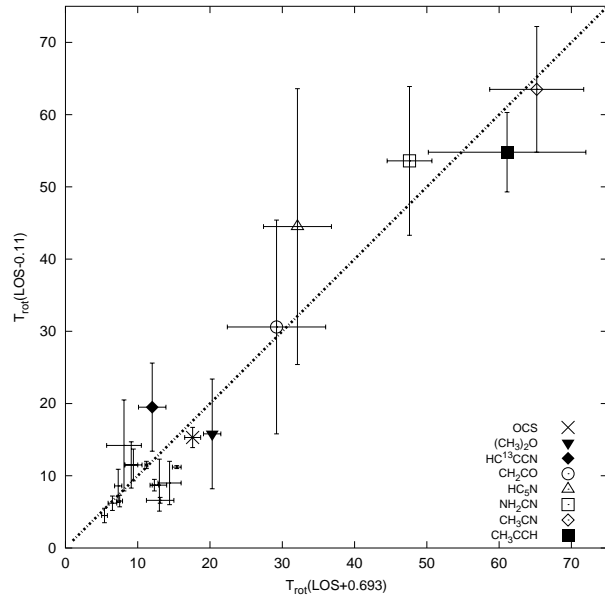


Figure 7. Relationship between the T_{rot} of both GC sources. The eight symbols show the highest T_{rot} measured in both GC sources. The dashed line shows the line of equal T_{rot} .

largest T_{rot} in our survey. We do not believe the high temperatures derived from CH₂CO and NH₂CN are biased by the range of the energy levels of the observed transitions. Although the HNCO RDs (see Fig. 5) cover the same range of energies than that of the NH₂CN, the derived T_{rot} for both molecules are very different. The wide range of derived T_{rot} for the different molecules does not seem to be due to difference in collisional cross sections, level structure and/or dipole moments. For NH₂CN and CH₂CO, which have virtually identical geometrical cross sections and level structure, but very different dipole moments ($\mu_a=4.32$ D for NH₂CN and $\mu_a=1.414$ D for CH₂CO) one would expect to observe a larger T_{rot} for CH₂CO. In contrast, NH₂CN shows a higher T_{rot} than CH₂CO.

Fig. 8 shows the molecular excitation (T_{rot}) derived for $LOS+0.693$ as a function of the dipole moment of the molecule. We found that there is not any clear dependence of T_{rot} with the dipole moment as expected if the emission from all molecules were arising from the same region.

Table 3. T_{rot} , column densities and abundances for both *LOS*s.

Molecule	<i>LOS</i> +0.693				<i>LOS</i> -0.11			
	V_{LSR} (σ) (km s ⁻¹)	T_{rot}^a (σ) (K)	N (σ) ($\times 10^{13}$ cm ⁻²)	N/N_{H_2} (σ) ($\times 10^{-9}$)	V_{LSR} (σ) (km s ⁻¹)	T_{rot}^a (σ) (K)	N (σ) ($\times 10^{13}$ cm ⁻²)	N/N_{H_2} (σ) ($\times 10^{-9}$)
¹³ CO	28100.0 (644.0) ^b	4810.0 (112.0)	11500.0 (953.0) ^b	4790.0 (566.0)
C ¹⁸ O	66.8 (0.3)	...	2344.2 (91.2) ^c	400.7 (22.0)	15.1 (0.6)	...	3010.0 (931.0) ^b	1260.0 (404.0)
C ¹⁷ O	65.7 (0.7)	...	489.8 (45.7) ^c	83.6 (8.5)	15.2 (3.7)	...	251.2 (77.6) ^c	105.2 (33.6)
CN	70.5 (0.5)	...	169.8 (17.4) ^d	29.0 (3.2)	13.9 (0.6)	...	173.8 (19.5) ^d	72.5 (10.1)
¹³ C ¹⁵ N ^e	67.9 (1.0)	...	67.6 (5.6) ^c	11.5 (1.1)	7.9 (2.0) ^d	3.3 (0.8)
¹³ CS	[45,80] ^g	...	2.3 (0.2) ^c	0.4 (0.04)	18.7 (0.2)	...	2.8 (0.1) ^c	1.2 (0.1)
SiO	9.0 (1.8) ^b	1.4 (0.2)	18.2 (0.2)	...	7.2 (0.2) ^c	3.0 (0.3)
²⁹ SiO	65.6 (0.6)	...	0.5 (0.1) ^c	0.09 (0.009)	21.8 (1.0)	...	0.9 (0.1) ^c	0.4 (0.1)
³⁰ SiO	71.8 (0.6)	...	0.5 (0.1) ^c	0.08 (0.009)	19.7 (0.5)	...	0.4 (0.03) ^c	0.2 (0.02)
SiS	69.5 (3.7)	...	4.5 (1.2) ^c	0.8 (0.2)	21.2 (1.1)	...	1.7 (0.4) ^c	0.7 (0.2)
SO	~68 ^f	8.1 (2.4)	61.0 (51.3)	10.4 (8.8)	~21 ^f	14.2 (8)	18.6 (3.7)	7.8 (2.0)
CCH	65.4 (0.4)	...	316.2 (18.6) ^d	54.1 (3.8)	19.8 (0.6)	...	251.2 (24) ^d	105.0 (13.3)
¹³ CCH	67.6 (2.4)	...	16.6 (3.5) ^d	2.8 (0.6)	27.9 (2.3)	...	11.1 (3.0) ^c	4.8 (1.3)
C ¹³ CH	60.6 (1.5)	...	14.8 (2.6) ^c	2.5 (0.5)	~8.7	~3.6
CCS	~67 ^f	7.3 (0.5)	5.6 (1.1)	1.0 (0.2)	~21 ^f	8.6 (2.3)	3.6 (2.3)	1.5 (1.0)
HCN	~240 ^b	~36	~480 ^b	~180
H ¹³ CN	~120 ^b	~12
...	~11 ^b	~2	~23 ^b	~9
...	~6 ^b	~1
HC ¹⁵ N	[40, 80] ^g	...	0.4 (0.04) ^c	0.06 (0.01)	[-0.8, 47.2] ^g	...	0.8 (0.1) ^c	0.3 (0.04)
...	[80, 110] ^g	...	0.2 (0.02) ^c	0.02 (0.01)
HCO	68.5 (1.3)	...	6.9 (1.4) ^d	1.2 (0.3)	~3.3	~1.4
HCS+	70.4 (0.7)	...	2.9 (0.3) ^c	0.5 (0.1)	21.8 (1.7)	...	1.4 (0.4) ^c	0.6 (0.2)
HNC	~240 ^b	~42	~180 ^b	~60
HN ¹³ C	~11 ^b	~2	~9 ^b	~3
H ¹⁵ NC	[40, 80] ^g	...	0.4 (0.05) ^c	0.07 (0.01)	21.5 (1.3)	...	0.3 (0.1) ^c	0.1 (0.01)
HNO	67.5 (0.8)	...	3.2 (0.4) ^c	0.6 (0.08)	17.2 (1.2)	...	2.5 (0.5) ^c	1.0 (0.2)
HOC ⁺	68.0 (0.8)	...	0.1 (0.01) ^c	0.02 (0.003)	~0.03	~0.01
HCO ⁺ , v=0,1,2	57.0 (1.3) ^b	9.6 (2.2)	36.0 (0.8) ^b	15.5 (3.0)
H ¹³ CO ⁺	2.7 (0.1) ^b	0.5 (0.1)	1.7 (0.04) ^b	0.7 (0.1)
HC ¹⁸ O ⁺	74.5 (2.8)	...	0.2 (0.1) ^c	0.04 (0.01)	23.4 (1.2)	...	0.2 (0.03) ^c	0.06 (0.01)
OCS	~65 ^f	17.6 (1.1)	186.2 (4.6)	31.8 (1.5)	~19 ^f	15.3 (1.4)	87.1 (14.1)	36.4 (6.5)
OC ³⁴ S	~66 ^f	12.1 (2.9)	21.4 (3.1)	3.7 (0.6)	~4.0	~1.7
O ¹³ CS	~66 ^f	11.3 (4.7)	7.8 (1.2)	1.3 (0.2)	~3.5	~1.5
O ¹³ C ³⁴ S	~3.0	~0.5
SO ₂	65.0 (0.4)	...	83.2 (3.4) ^c	14.2 (1.0)	18.6 (1.0)	...	20.4 (3.7) ^c	8.6 (1.7)
HNCO	~66 ^f	11.2 (0.2)	144.5 (5.6)	24.7 (1.4)	~18 ^f	11.5 (0.5)	67.6 (4.5)	28.3 (3.0)
H ¹⁵ NCO	~0.4	~0.1	~0.3	~0.1
HNC ¹⁸ O	~1.1	~0.2	~0.9	~0.4
HNCS, a-type	~66 ^f	15.2 (5.6)	3.1 (2.2)	0.5 (0.4)	21.2 (2.0)	...	2.0 (0.6) ^c	0.8 (0.3)
HOCO ⁺	~66 ^f	7.5 (0.4)	12.0 (1.4)	2.1 (0.3)	~20 ^f	6.5 (0.8)	4.8 (1.2)	2.0 (0.6)
CH ₂ CO	~66 ^f	29.2 (6.8)	22.9 (6.8)	3.9 (1.2)	~19 ^f	30.6 (14.8)	14.8 (12.3)	6.2 (5.2)
CH ₂ NH	71.5 (1.0)	...	29.5 (4.8) ^c	5.0 (0.8)	17.8 (2.6)	...	24.0 (7.8) ^c	10.1 (3.4)
HC ₃ N	~70 ^f	15.4 (0.6)	54.9 (3.3) ^b	9.4 (1.0)	~18 ^f	11.2 (0.2)	26.8 (0.6)	11.2 (1.0)
H ¹³ CCCN	~70 ^f	14.4 (1.6)	2.6 (0.2)	0.5 (0.03)	~18 ^f	9.0 (3.0)	1.9 (0.3)	0.8 (0.2)
HC ¹³ CCN	~66 ^f	12.0 (1.9)	2.0 (0.2)	0.4 (0.04)	~20 ^f	19.5 (6.1)	1.3 (0.4)	0.5 (0.2)
HCC ¹³ CN	~68 ^f	9.4 (1.2)	2.7 (0.5)	0.5 (0.10)	~19 ^f	11.5 (2.2)	1.4 (0.3)	0.6 (0.1)
HCCNC	70.1 (3.1)	...	0.7 (0.3) ^c	0.1 (0.05)	~0.9	~0.4
HCOOH	~67 ^f	18.9 (4.8)	14.4 (6.2)	2.5 (1.1)	18.6 (0.9)	...	15.9 (4.2) ^d	6.6 (1.8)
H ₂ C ₂ N	70.4 (0.7)	...	11.0 (1.4) ^d	1.9 (0.3)	17.6 (1.2)	...	4.8 (1.2) ^d	2.0 (0.5)
NH ₂ CN	~67 ^f	47.6 (3.1)	11.9 (1.5)	2.0 (0.3)	~20 ^f	53.6 (10.3)	8.3 (3.0)	3.5 (1.3)
c-C ₃ H ₂	~69 ^f	13.1 (1.9)	9.4 (2.5)	1.6 (0.4)	~20 ^f	6.6 (0.4)	6.0 (0.7)	2.5 (0.4)
CH ₃ CN, v8=0,1	69.7 (0.8)	65.2 (6.5)	28.0 (3.0) ^b	4.8 (0.6)	~20 ^f	63.5 (8.7)	7.4 (1.6)	3.1 (0.7)
¹³ CH ₃ CN	~74 ^f	73.3 (32.2)	1.1 (0.7)	0.2 (0.1)	...	63.5	~1.5	~0.6
CH ₃ ¹³ CN	69.7 (0.8)	73.3	1.4 (0.2) ^d	0.2 (0.03)	...	63.5	~1.9	~0.8
CH ₃ OH	12700.0 (1420.0) ^b	2160.0 (257.0)	...	13.0	~3981.0	~1670.0
¹³ CH ₃ OH	70.4 (1.9)	14.0	602.6 (67.6) ^c	103.0 (12.2)	...	13.0	~758.6	~317.7
NH ₂ CHO	~68 ^f	12.3 (0.6)	5.9 (0.6)	1.0 (0.1)	~19 ^f	8.7 (0.8)	2.5 (0.5)	1.0 (0.2)
C ₂ H ₃ CN	~70 ^f	9.1 (0.9)	5.1 (1.6)	0.9 (0.3)	~20 ^f	11.5 (3.2)	2.0 (1.3)	0.8 (0.5)
CH ₃ CCH	~68 ^f	61.1 (10.9)	262.4 (16.9)	44.9 (3.4)	~21 ^f	54.8 (5.5)	74.1 (12.3)	31.0 (5.8)
CH ₃ ¹³ CCH	80.9 (2.2)	61.1	12.6 (3.9) ^d	2.2 (0.7)	...	54.8	~12.8	~5.4
CH ₃ CHO-A	~69 ^f	5.4 (0.4)	49.0 (10.2)	8.4 (1.8)	~17 ^f	4.5 (1.0)	12.0 (9.1)	5.0 (3.8)
CH ₃ CHO-E	~72 ^f	6.5 (0.6)	15.9 (5.0)	2.7 (0.9)	~21 ^f	6.2 (1.0)	20.9 (8.5)	8.8 (3.6)
HC ₅ N	~66 ^f	32.1 (4.7)	3.5 (1.2)	0.6 (0.2)	~20 ^f	44.5 (19.1)	2.2 (1.8)	0.9 (0.8)
CH ₃ COOH-E	~4.0	~0.7	~4.3	~1.8
CH ₃ OCHO-A	~69 ^f	11.5 (1.0)	34.7 (7.4)	5.9 (1.3)	~19.8	~8.3
CH ₃ OCHO-E	~70 ^f	11.9 (1.1)	36.3 (7.4)	6.2 (1.3)	17.7 (2.1)	...	23.4 (10) ^c	9.8 (4.2)

Molecule	LOS+0.693				LOS-0.11			
	V _{LSR} (σ) (km s ⁻¹)	T _{rot} ^a (σ) (K)	N (σ) (×10 ¹³ cm ⁻²)	N/N _{H2} (σ) (×10 ⁻⁹)	V _{LSR} (σ) (km s ⁻¹)	T _{rot} ^a (σ) (K)	N (σ) (×10 ¹³ cm ⁻²)	N/N _{H2} (σ) (×10 ⁻⁹)
HCOCH ₂ OH	73.8 (0.9)	...	6.5 (5.6) ^c	1.1 (1.0)	≤4.8	≤2.0
C ₂ H ₅ CN	~67 ^f	13.0 (1.0)	8.1 (1.6)	1.4 (0.3)	~18 ^f	8.7 (3.6)	4.8 (3.2)	2.0 (1.4)
(CH ₃) ₂ O	~72 ^f	20.3 (1.2)	91.2 (10.0)	15.5 (1.6)	~19 ^f	15.8 (7.6)	63.1 (50.1)	26.4 (21.1)
C ₂ H ₅ OH	~68 ^f	5.3 (0.4)	44.7 (8.7)	7.6 (1.5)	18.6 (0.5)	...	25.1 (2.5) ^d	10.5 (1.4)

^a T_{rot} derived from RDs or assumed for deriving molecular column densities. The assumed T_{rot} for the ¹³C isotopologues of CH₃CCH and CH₃CN are taken from their other isotopologues. The assumed T_{rot} for the CH₃OH and its ¹³C isotopologue are taken from Requena-Torres et al. (2008). The T_{rot} quoted with uncertainties are determined from RDs. When the T_{rot} is not listed means that a T_{rot} of 10 K is assumed, which corresponds to an average value of the low T_{rot} component derived from other molecules by using RDs.

^b We have inferred from the ¹²C/¹³C ≤ 15, ¹⁴N/¹⁵N ≤ 280 and ¹⁶O/¹⁸O ≤ 186 isotopic ratios given in Table 4 that the column density of the most abundant isotopologues of this molecule are biased by opacity/self-absorption. Thus here we have derived the column density by using either its ¹⁸O, ¹⁵N or ¹³C isotopologue for its respective velocity component and assuming the ¹⁶O/¹⁸O = 250 or ¹⁴N/¹⁵N > 600 ratios (W&R94) and if necessary our ¹²C/¹³C = 21 ratio. For LOS+0.693 the SiO column density is derived from the ²⁸SiO isotopologue assuming a ²⁸Si/³⁰Si ratio of 18 derived in LOS-0.11.

^c Only one line of this molecule is detected.

^d Although several transitions of this molecule are detected, there is an insufficient dynamical range in *E_u* in order to derive the column density from a RD, then we have chosen one transition (see note cd in Tables 1 and 2), usually the less affected by opacity.

^e The observed transition is contaminated by the emission from an unknown molecular species.

^f This velocity is an average of different detected transitions.

^g These velocity ranges are chosen for deriving velocity-integrated intensities used in the molecular column density estimate. For LOS+0.693 we have used a velocity range for the ¹³CS(2-1) line as it is affected by opacity/self-absorption. For the ¹⁵N isotopologues of HNC and HCN the velocity ranges are suitable for deriving ¹⁴N/¹⁵N ratios (see text).

Table 4. Isotopic ratios for both GC lines of sight.

Isotope	molecular column density ratio	MC+0.693		MC-0.11	Bibliographic Data ^a
		V _{LSR} (km s ⁻¹) ~68	~85	V _{LSR} (km s ⁻¹) ~20	
Ratios/limits unbiased by opacity/self-absorption in both GC sources					
¹² C/ ¹³ C	CN: ¹³ CN	22.9 (4.7)	...	21.2 (5.7)	~20
	CCH: ¹³ CCH	19.1 (4.1)	...	22.6 (6.5)	
	CCH:C ¹³ CH	21.4 (3.9)	...	≥29	
	OCS:O ¹³ CS	22.8 (3.8)	...	≥25	
	CH ₃ CCH:CH ¹³ CCH	20.8 (6.6)	...	≥6	
¹⁴ N/ ¹⁵ N	HNCO:H ¹⁵ NCO	≥380	...	≥214	>600
¹⁸ O/ ¹⁷ O	C ¹⁸ O:C ¹⁷ O	4.8 (0.5)	...	2.6 (0.9)	3.2 (0.2)
¹⁶ O/ ¹⁸ O	HNCO:HNC ¹⁸ O	≥129	...	≥78	250
²⁹ Si/ ³⁰ Si	²⁹ SiO: ³⁰ SiO	1.1 (0.2)	...	2.2 (0.4)	1.5
Ratios/limits biased by opacity/self-absorption/ripples in one/both GC sources					
¹² C/ ¹³ C	HCN:H ¹³ CN	4.5 (0.7) ^b	5.1 (0.7)	4.4 (0.1) ^c	~20
	HNC:HN ¹³ C	3.0 (0.4) ^b	...	5.1 (0.3)	
	HCO ⁺ :H ¹³ CO ⁺	5.0 (0.7) ^b	6.8 (1.0)	7.1 (0.2) ^c	
	HC ₃ N:H ¹³ CCCN	11.6 (0.8)	...	13.9 (2.4)	
	HC ₃ N:HC ¹³ CCN	14.8 (1.5)	...	21.1 (6.1)	
	HC ₃ N:HCC ¹³ CN	11.0 (2.1)	...	20.0 (4.7)	
	CH ₃ OH: ¹³ CH ₃ OH	15.1 (3.8)	
	CH ₃ CN: ¹³ CH ₃ CN	13.6 (9.1)	...	≥5	
	CH ₃ CN:CH ¹³ CN	10.9 (1.6)	...	≥4	
	¹⁴ N/ ¹⁵ N	¹² C: ¹³ C×HN ¹³ C:H ¹⁵ NC	148.7 (23.4) ^{d,e}	...	280.8 (25.2) ^e
¹⁶ O/ ¹⁸ O	¹² C: ¹³ C×H ¹³ CN:HC ¹⁵ N	100.5 (14.7) ^{d,e}	163.0 (23.1) ^d	141.8 (17.3) ^e	
	¹² C: ¹³ C× ¹³ C ¹³ CO:C ¹⁸ O	136.3 (7.2) ^e	...	185.5 (17.0) ^e	250
³² S/ ³⁴ S	OCS:OC ³⁴ S	8.7 (1.3) ^f	...	≥22	~22
	¹² C: ¹³ C×O ¹³ CS:OC ³⁴ S	7.7 (1.6) ^{e,f}	
	O ¹³ CS:O ¹³ C ³⁴ S	≥3	

^a Isotopic ratios from W&R94.

^b The ¹²C and ¹³C isotopologues are affected by opacity/self-absorption.

^c The ¹²C isotopologue is affected by opacity/self-absorption.

^d The ¹³C isotopologue is affected by opacity/self-absorption.

^e We have averaged the ¹²C/¹³C isotopic ratios unbiased by opacity/self-absorption, then we have obtained the average ¹²C/¹³C ~ 21 ratio over both GC sources. In these ratios we have used the ¹²C/¹³C = 21 ratio.

^f The OC³⁴S lines are affected by ripples.

Although the origin of the difference in T_{rot} is uncertain, we postulate that it may be related to the formation of the molecular species. In the shock scenario proposed by Requena-Torres et al. (2006) and Martín et al. (2008), the molecular species showing higher T_{rot} will be those produced at early times or just ejected from grain and those with lower T_{rot} should be located in the post shocked regions.

4.1.2 Starburst galaxies

The bulk of the quiescent molecular clouds in the GC seem to show rather uniform physical conditions and chemical composition. In this section we compare our results obtained for the GC clouds with those derived for nearby extragalactic nuclei with different type of activity. Table 5 summarizes the T_{rot} and molecular abundances of selected species

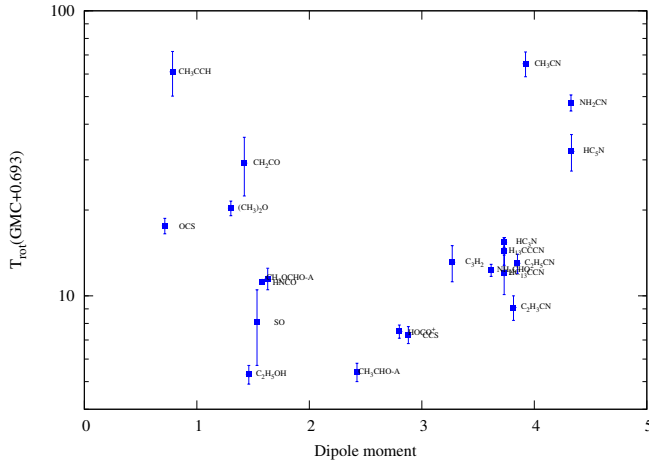


Figure 8. The molecular dipole moments represented as a function of the T_{rot} derived for $LOS+0.693$. CH_3CN and CH_3CCH are the molecules that show the highest T_{rot} in this survey. When any molecule has more than one dipole moment we have represented the highest value.

derived for both GC sources and four extragalactic nuclei, NGC 253, M 82, IC 342 and Maffei 2. The molecular species selected in Table 5 and their corresponding T_{rot} has been successfully used by Martín et al. (2009a) and Aladro et al. (2011a) to study the evolution of the nuclei of starburst galaxies. Based on the excitation and the molecular abundances, Martín et al. (2009a) and Aladro et al. (2011a) have classified Maffei 2 as a young starburst galaxy, IC 342 and NGC 253 as intermediate-age starburst galaxies and M 82 as an evolved starburst galaxy (Aladro et al. 2011a).

In column 8 of Table 5, we show the ratio between the molecular abundance of $LOS-0.11$ and those of $LOS+0.63$ and the nuclei of nearby galaxies. While the molecular abundances in the two GC LOS s clouds are within a factor of 3, those in galactic nuclei are, for most molecules, at least one order of magnitude smaller than those measured in the GC. This is expected since the volume sampled in external galaxies is, at least, four orders of magnitude larger than in the GC. Then the ratio between diffuse molecular gas measured by the H_2 column densities to dense gas traced by other species is smaller in the GC than in external galaxies. However, some molecular species show changes in their abundances by more than one order of magnitude relative to high density tracers like CS. In particular, CH_3OH shows the lowest abundances in galaxies like M 82, IC 342 and Maffei 2 by factors of $\sim(1-6) \times 10^2$ relative to $LOS-0.11$. NGC 253 is the galaxy that shows the highest methanol abundance between the starburst galaxies in our sample. The radiation field in NGC 253 seems to be higher than in M 82, IC 342 and Maffei 2 (Carral et al. 1994; Israel & Baas 2003). However, differences in the evolutionary stage of the starbursts and molecular clouds (Aladro et al. 2011a), the distribution of star forming regions and/or the strength of large-scale shocks could be responsible for the high methanol abundance in NGC 253 as compared to those of the other galaxies in our sample. Similar lower methanol abundances, by nearly two orders of magnitude, are also observed toward a sample of molecular clouds in the GC (Requena-Torres et al. 2006) that are affected by the UV photodissociation from HII re-

gions. This suggests that this molecule is likely photodissociated by the strong UV radiation field of $G_0 \sim 10^{2.5-4.0}$ (Carral et al. 1994; Israel & Baas 2003) present in these nearby galaxies considered in this comparison.

Another molecule which also shows large abundance differences between our sample of galaxies and $LOS-0.11$ is HNC. It is expected that gas-phase HNC survives in well-shielded dense molecular clouds, while it is photodissociated in unshielded regions affected by UV radiation (Martín et al. 2008). The high HNC abundances derived in both GC sources compared to those found in the starburst galaxies NGC 253 and M 82 support the idea that HNC is a suitable tracer of dense molecular gas ($\gtrsim 10^6 \text{ cm}^{-3}$) in clouds unaffected by strong UV radiation (Martín et al. 2008). This agrees with the finding of Amo-Baladrón et al. (2011), who found that the HNC abundance in the 20 km s^{-1} cloud dominated by shocks is a factor of 20 higher than in the CND surrounding Sgr A* which is affected by both shocks and photodissociation.

The photodissociation rate of HNC is a factor of ~ 1.5 larger than that of CH_3OH . Both molecules have photodissociation rates higher (a factor ~ 3) and lower (a factor ~ 4) than those of CCH and HC_3N , respectively. The smaller differences found in the CCH abundances compared to those of CH_3OH and HNC between $LOS-0.11$ and the starburst galaxies M 82 and NGC 253 is likely due to the differences in the photodissociation rates of these molecules. Additionally, CCH could increase its abundance efficiently in PDRs (Mul & McGowan 1980). One expects that HC_3N would show larger abundance variations than CH_3OH and HNC between $LOS-0.11$ and both starburst galaxies due to their differences in the photodissociation rates. However, this is not observed in Table 5. Efficient formation of HC_3N through ion-molecule chemistry (Knight et al. 1986) could be responsible for the high HC_3N abundance found in both starburst galaxies. The largest differences shown by CH_3OH and HNC in our comparison is likely due to their photodissociation and that both molecules are not expected to form efficiently in gas phase. CH_3OH shows higher differences in its abundance than HNC between $LOS-0.11$ and the starburst galaxies in our sample. This is probably due to the higher extinction of the dense clouds, cores where HNC arises ($\gtrsim 10^6 \text{ cm}^{-3}$, Martín et al. (2008)) as compared with the more diffuse conditions where CH_3OH is found ($\sim 5 \times 10^4 \text{ cm}^{-3}$, Martín et al. (2006a)).

Overall, complex molecules in the molecular clouds of this sample of starburst galaxies reveal smaller abundances than those measured in the GC sources by nearly 2 orders of magnitude, suggesting that a substantial fraction of the molecular gas in the nearby galaxies in our sample is affected by photodissociation by the UV radiation from the starburst.

Fig. 9 shows the T_{rot} of selected molecules derived in NGC 253 (Martín et al. 2006b; Aladro et al. 2011a) and M 82 (Aladro et al. 2011b) versus the T_{rot} derived for $LOS-0.11$. In contrast to the large abundance difference found between the GC clouds and starburst galaxies, the excitation of complex molecules like $c\text{-C}_3\text{H}_2$, HC_3N and CH_3OH derived for both starburst galaxies, NGC 253 and M 82, is similar within $\sim 3\sigma$ to the excitation of the molecular cloud found for $LOS-0.11$. Like in the two LOS s in the GC, NH_2CN and CH_3CCH in NGC 253 also show high

Table 5. Abundance and excitation of galactic and extragalactic sources.

Source name and Nominal positions J2000 (α, β)	Type	Molecule	T_{rot} (σ) (K)	N_{H_2} (σ) (cm^{-2})	N (σ) ($\times 10^{13} cm^{-2}$)	$X=N/N_{H_2}$ $\times 10^{-9}$	$(X_1/X)^A$
<i>LOS</i> +0.693 17 ^h 47 ^m 22 ^s 0, -28°21′27″0	Molecular cloud	CS	10.0	5.9 (0.2) $\times 10^{22}$	48.3 (4.2) ^B	8.2 (1.0)	3.0 (0.4)
		SO	8.1 (2.4)		61.0 (51.3)	10.3 (8.7)	0.8 (0.6)
		SiO	10.0		9.0 (1.8)	1.4 (0.2)	2.1 (0.3)
		OCS	17.6 (1.1)		186.2 (4.6)	31.6 (1.5)	1.2 (0.2)
		CCH	10.0		316.2 (18.6)	53.6 (3.8)	2.0 (0.3)
		HCO ⁺	10.0		57.0 (1.3)	9.6 (2.2)	1.6 (0.5)
		HNCO	11.2 (0.2)		144.5 (5.6)	24.5 (1.3)	1.2 (0.1)
		HC ₃ N	15.4 (0.6)		54.9 (3.3)	9.4 (1.0)	1.2 (0.1)
		CH ₃ OH	14.0 (1.3) ^a		12700.0 (1420.3)	2160.0 (255.0)	0.5 (0.1)
		CH ₃ CCH	61.1 (10.9)		262.4 (16.9)	44.5 (3.3)	0.7 (0.1)
<i>LOS</i> -0.11 17 ^h 45 ^m 39 ^s 3, -29°04′05″0	Molecular cloud	CS	10.0	2.4 (0.2) $\times 10^{22}$	58.8 (2.1) ^B	24.5 (2.2)	1
		SO	14.2		18.6 (3.7)	7.8 (2.0)	1
		SiO	10.0		7.2 (0.2)	3.0 (0.3)	1
		OCS	15.3 (1.4)		87.1 (14.1)	36.3 (6.6)	1
		CCH	10.0		251.2 (24.0)	104.7 (13.2)	1
		HCO ⁺	10.0		36.0 (0.8)	15.5 (3.0)	1
		HNCO	11.5 (0.5)		67.6 (4.5)	28.2 (3.0)	1
		HC ₃ N	11.2 (0.2)		26.8 (0.6)	11.2 (1.0)	1
		CH ₃ OH	13.0 (1.0) ^a		...	1100.0 (220) ^{a,C}	1
		CH ₃ CCH	54.8 (5.5)		74.1 (12.3)	30.9 (5.7)	1
NGC 253 00 ^h 47 ^m 33 ^s 3, -25°17′23″0	Intermediate-age starburst	CS	12.0 (3) ^b	6.2 (0.5) $\times 10^{22b}$	15.0 (6.0) ^b	2.4 (1.0)	10.2 (4.2)
		SO	40 (24) ^c		4.5 (3.3) ^c	0.73 (0.5)	10.7 (7.9)
		SiO	7.4 (0.7) ^c		0.5 (0.1) ^c	0.081 (0.02)	37.0 (8.7)
		OCS	17 (2) ^c		25.0 (3.0) ^c	4.0 (0.6)	9.1 (2.0)
		CCH	10.0 ^d		73.0 (1.0) ^d	11.8 (1.0)	8.9 (1.3)
		HNCO	23.0 (6.0) ^c		5.7 (2.7) ^c	0.9 (0.4)	31.3 (15.0)
		HC ₃ N	11.6 (1.8) ^b		8.1 (2.9) ^b	1.3 (0.5)	8.6 (3.2)
		CH ₃ OH	11.6 (0.2) ^c		83 (3) ^c	13.4 (1.2)	82.1 (18.0)
		CH ₃ CCH	44.4 (7.7) ^b		32.0 (10.0) ^b	5.2 (1.7)	5.9 (2.2)
		CS	15.1 (0.9) ^b		3.6 (0.5) ^b	0.5 (0.1)	49.0 (9.3)
M 82 09 ^h 55 ^m 51 ^s 9, 69°40′47″1	Evolved starburst	CCH	10.0 ^{e,D}	7.9 (0.4) $\times 10^{22b}$	55.0 (1.0) ^{e,D}	6.5 (0.4) ^D	16.1 (2.2)
		HNCO	10.0 ^{f,D}		$\lesssim 0.7f,D$	$\lesssim 0.1D$	$\gtrsim 282$
		HC ₃ N	24.7 (3.9) ^b		2.5 (1.1) ^b	0.3 (0.1)	37.3 (16.0)
		CH ₃ OH	4.5 ^f		15.0 ^f	1.9	579.0
		CH ₃ CCH	28.1 (1.2) ^b		85.0 (9.0) ^b	10.8 (1.3)	2.9 (0.6)
		CS	10.6 (0.2) ^b		6.0 (0.1) ^b	1.0 (0.1)	24.5 (2.6)
		SO	$\gtrsim 0.08g,E$	$\gtrsim 1.1$
		CCH	0.3 ^{g,E}	3.5
		HNCO	10.2 (0.4) ^e		12.0 (1.0) ^e	2.1 (0.2)	13.4 (2.0)
		HC ₃ N	13.1 (2.3) ^b		2.7 (1.1) ^b	0.5 (0.2)	22.4 (10.0)
IC 342 03 ^h 46 ^m 48 ^s 5, 68°05′46″0	Intermediate-age starburst	CH ₃ OH	...	5.8 (0.4) $\times 10^{22b}$...	5 ^{g,E}	220
		CH ₃ CCH	70.0 ^b		45.0 ^b	7.8	4.0
		CS	9.7 (8.1) ^b		6.9 (5.7) ^b	1.6 (1.3)	15.3 (13.3)
		SiO	0.08 ^{h,E}	36.2
		CCH	9.6 ^{h,E}	10.9
		HCO ⁺	3.5 ^{h,E}	4.4
		HNCO	11.5 (0.6) ^e		10 (2) ^e	2.3 (0.6)	12.3 (3.6)
		HC ₃ N	11.6 (0.8) ^b		4.3 (0.6) ^b	1.0 (0.2)	11.2 (2.8)
		CH ₃ OH	10.0 ^f		33.0 ^f	7.5	147.0
		CH ₃ CCH	$\lesssim 46.9b$		$\lesssim 11b$	$\lesssim 2.5$	$\gtrsim 12.4$
Maffei 2 02 ^h 41 ^m 55 ^s 1, 59°36′15″0	Young starburst	CS	9.7 (8.1) ^b	4.4 (0.8) $\times 10^{22b}$	6.9 (5.7) ^b	1.6 (1.3)	15.3 (13.3)
		SiO	0.08 ^{h,E}	36.2
		CCH	9.6 ^{h,E}	10.9
		HCO ⁺	3.5 ^{h,E}	4.4
		HNCO	11.5 (0.6) ^e		10 (2) ^e	2.3 (0.6)	12.3 (3.6)
		HC ₃ N	11.6 (0.8) ^b		4.3 (0.6) ^b	1.0 (0.2)	11.2 (2.8)
		CH ₃ OH	10.0 ^f		33.0 ^f	7.5	147.0
		CH ₃ CCH	$\lesssim 46.9b$		$\lesssim 11b$	$\lesssim 2.5$	$\gtrsim 12.4$

Notes : A-Ratio between the molecular abundances for *LOS*-0.11 and those for the other sources in this table; B-The CS abundances for both GC sources are derived from the ¹³CS abundances by using our ¹²C/¹³C=21 ratio; C-An uncertainty of 20% in the methanol abundance is assumed; D-Offset position of 13″0, 7″5 relative to 09^h55^m51^s9, 69°40′47″1 (J2000) with $N_{H_2}=8.5\times 10^{22} cm^{-2}$ (Martín et al. 2006a). E-This abundance corresponds to the cloud A in IC 342 or cloud F in Maffei 2, both clouds are located in projection close to the nuclear star clusters. Uncertainties in the abundances are at least a factor of 3.

^a Requena-Torres et al. (2008).

^b Aladro et al. (2011a).

^c Martín et al. (2006b).

^d Martín et al. (2010).

^e Martín et al. (2009a).

^f Martín et al. (2006a).

^g Meier & Turner (2005).

^h Meier & Turner (2012).

T_{rot} of 67 K and 44 K, respectively. Interestingly these T_{rot} are within a factor of 1.2 of those of NGC 253. In M 82, the T_{rot} derived from CH₃CCH and CH₃CN show the same trend than in NGC 253 but in this case they are a factor of ~ 2 lower than those observed in *LOS*-0.11. It is remarkable that the excitation of molecular clouds in the nuclei of galaxies with different activity and evolutionary stage appears relatively uniform, suggesting that the physical conditions,

H₂ densities and kinetic temperatures, must be very similar. If, as suggested in the previous section, the excitation of the molecules is related to the formation mechanism, there must be a common processes driving the chemistry in the nuclei of galaxies. However, to explain the underabundance of CS, HC₃N, CH₃OH, HNCO and other molecules (see Table 5) found in our sample of galactic nuclei with respect to the GC, the shock scenario proposed by Requena-Torres et al.

(2006) and Martín et al. (2008) for the GC must be combined with the effects of the photodissociation as proposed by Aladro et al. (2011b).

4.2 Tracing the UV and X-ray induced chemistry in galactic nuclei

The scenario proposed in the previous section to explain the difference in abundance ratios between these quiescent Galactic center *LOS*s and our sample of galactic nuclei would indicate that the clouds in the two *LOS*s are only marginally affected by the UV radiation. However, in our survey we have detected, for the first time, HCO and HOC⁺ emission toward *LOS*+0.693 in the GC. Emission from these molecules are considered to be tracers of UV and X-ray induced chemistry in the associated PDRs (Apponi et al. 1999; Goicoechea et al. 2009; Martín et al. 2009b) and XDRs (Usero et al. 2004; Spaans & Meijerink 2007). It has been proposed that abundance and abundance ratios between key molecules like HCO, HOC⁺ and HCO⁺ can be used to trace the XDR and PDR chemistries and even to differentiate between them (Meijerink et al. 2007; Spaans & Meijerink 2007). The high spatial resolution of our data offers an unique opportunity to study the PDR/XDR component in nuclei of galaxies using molecular tracers.

4.2.1 Constrains on the X-ray radiation in the molecular clouds along the GC *LOS*

Fig. 10 illustrates the key difference in the X-ray emission observed toward the two *LOS*s (shown as open circles) in the GC. While *LOS*−0.11 only shows continuum emission in the 0.1–10 keV band, *LOS*+0.693 shows, in addition to the continuum emission, one of the strongest Fe K α (6.4 keV) lines observed in our Galaxy (Koyama et al. 1996). The presence of the strong Fe K α line emission is considered as an excellent tracer of XDRs (Martín-Pintado et al. 2000), showing that X-rays are directly interacting with large column densities of matter. As a consequence of this interaction one would expect a chemistry driven by X-rays. In contrast, *LOS*−0.11 does not show any emission of the Fe K α line (Ponti et al. 2010), indicating the lack of any relevant XDR.

4.2.2 Constrains on the UV radiation in the molecular clouds along the GC *LOS*

As shown in Fig. 1, the two *LOS*s do not show any prominent HII region which would produce associated PDRs. However, *LOS*+0.693 is relatively close to the HII regions of Sgr B2N and L, whereas *LOS*−0.11 is located near the non-thermal sources Sgr A-E and Sgr-F (Lu et al. 2003; Yusef-Zadeh et al. 2005). We can use the upper limit to the H α recombination line emission in our survey to constrain the Lyman photons in the beam. None of the four H α , H39 α to H43 α , recombination lines that fall in the frequency range of our spectral line survey are detected toward both *LOS*s. From the 3σ upper limit to their intensities and assuming a linewidth of ~ 35 km s^{−1}, we have set the upper limits to the thermal continuum fluxes given in Table 6. For optically thin emission and the average LTE electron temperature of 6500 K estimated toward the GC (Goss et al. 1985), we

have derived the upper limits to the Lyman continuum photons (Mezger & Henderson 1967) given in Table 6. These upper limits of $\lesssim 10^{48.4}$ and $\lesssim 10^{48.7}$ s^{−1} for *LOS*+0.693 and *LOS*−0.11, respectively, would constrain the spectral type of any ionizing star to be later than O8–O9.

Low angular resolution observations of fine structure lines of CII and OI toward Sgr B2 have shown the presence of an extended FUV radiation field of $G_0 \approx 10^3$ – 10^4 , which should produce important PDRs. However, this FUV radiation field would be characterized by a Lyman continuum photon flux of $\sim 10^{50.4}$ s^{−1} (Goicoechea et al. 2004). This flux is ~ 50 times larger than that derived from the recombination lines in *LOS*+0.693. Given the large difference in beam size between our observations and those of the fine structure lines, it is possible that inhomogeneities in the FUV radiation field could partially explain this discrepancy. In any case, the UV radiation field strength of the PDR component in *LOS*+0.693 is rather uncertain. The situation for *LOS*−0.11 seems to be simpler since there is not nearby massive star formation, like Sgr B2N, which could provide a large FUV radiation field. In this *LOS* one expects a negligible PDR component.

4.2.3 The HCO, HOC⁺, HCO⁺ and CS abundance as tracers of the PDR and XDR components in galactic nuclei

Table 7 shows the HCO⁺/HOC⁺, HCO⁺/HCO and HCO/HOC⁺ ratios measured for our two *LOS*s, the extragalactic sources (NGC 253, M 82 and NGC 1068) and typical galactic PDRs. The HCO⁺ column densities were calculated from the HC¹⁸O⁺ line by assuming $^{16}\text{O}/^{18}\text{O}=250$ (W&R94). We also have included abundances of CS relative to HOC⁺ and HCO since the CS abundance does not seem to change substantially in PDRs and shocked environments in the GC (Requena-Torres et al. 2006; Martín et al. 2008).

4.2.4 The CS/HOC⁺ and CS/HCO ratios

Both *LOS*s in the GC show CS/HOC⁺ ratios which are larger than those measured in Galactic PDRs and galaxies by factors of $\gtrsim 4$ and $\gtrsim 15$, respectively, except for that of the molecular peak of the Orion Bar, which is completely shielded from UV radiation. Although the CS/HCO ratios also show the same trend as CS/HOC⁺, the CS/HCO ratios are less conclusive since these ratios are within a factor of ~ 3 for all kinds of objects. This suggests that the PDR/XDR component, traced by HOC⁺ and to a lesser extent by HCO in both *LOS*s of the GC is smaller than those in starburst galaxies and typical unshielded galactic PDRs. The larger CS/HOC⁺ ratio found in *LOS*−0.11 than in *LOS*+0.693 suggests a very small (basically negligible) XDR/PDR component along *LOS*−0.11. This is consistent with the measurements of UV and X-ray emission toward these *LOS*s shown in Fig. 1 and 10, respectively. The CS/HOC⁺ ratios measured in external galaxies are also consistent with this ratio being a good tracer of the PDR/XDR component relative to the total gas (see Table 7). The most evolved starburst M 82, has the lowest CS/HOC⁺ ratio (1), consistent with its classification as a PDR dominated galaxy while NGC 253 an intermediate-age starburst has a larger CS/HOC⁺ ratio

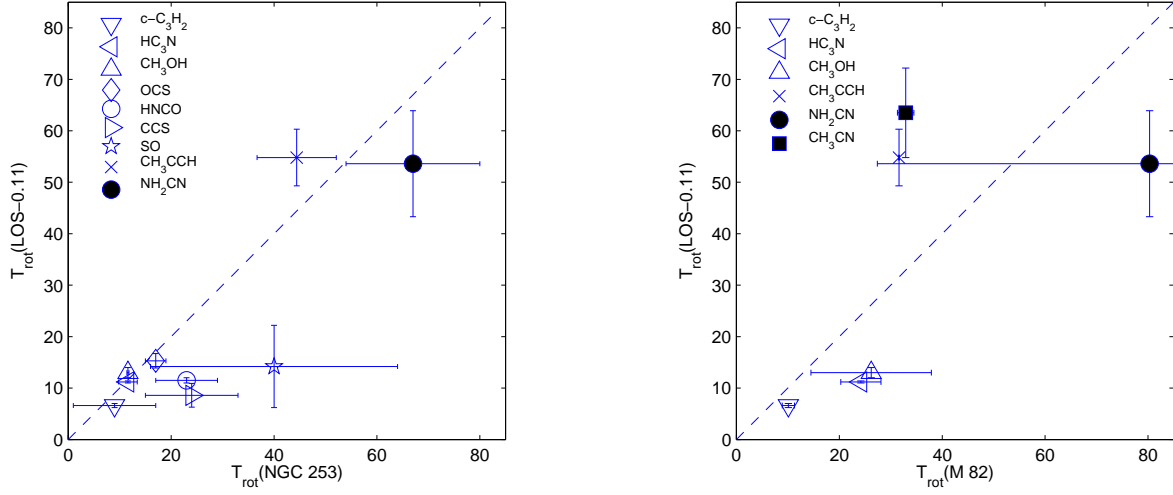


Figure 9. Relationship between the T_{rot} of NGC 253 (left) and M 82 (right) with the T_{rot} of $LOS-0.11$. Different symbols correspond to different molecules. The T_{rot} for NGC 253 are taken from Martín et al. (2006b) and Aladro et al. (2011a), and for M 82 from Aladro et al. (2011b). For $LOS-0.11$, the T_{rot} of methanol is taken from Requena-Torres et al. (2008). The dashed line on each plot is the line of equal T_{rot} .

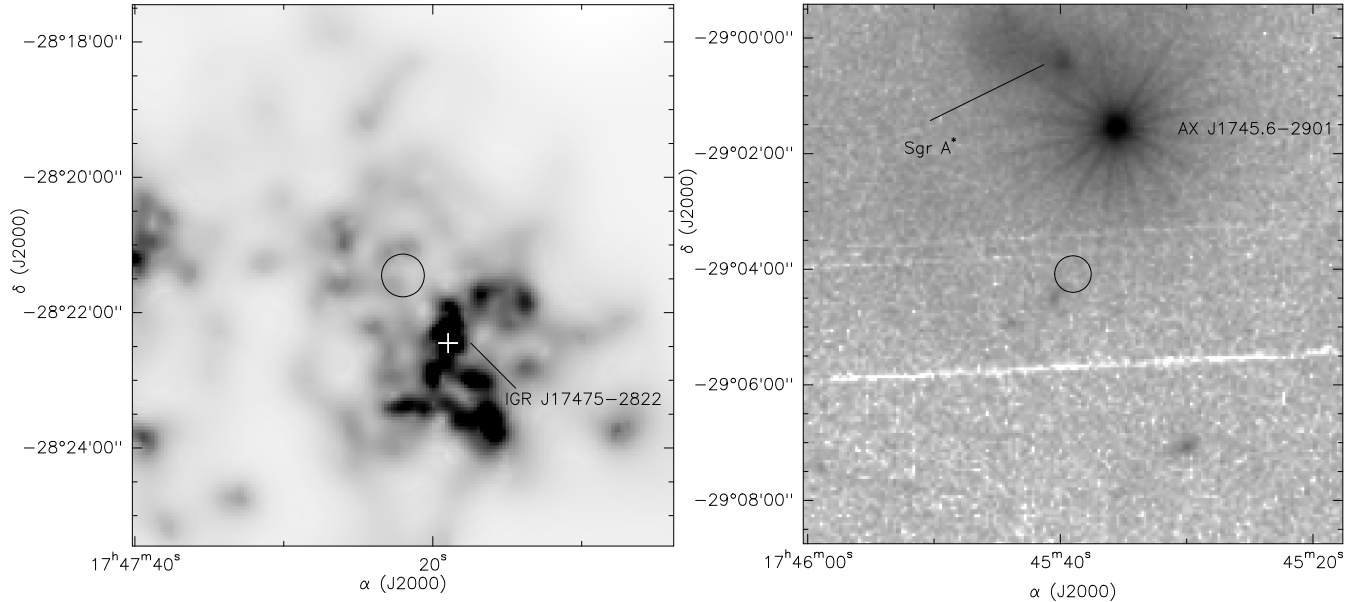


Figure 10. (Left panel) Fe $K\alpha$ line emission observed with the XMM Newton satellite in 2001-2004 toward Sgr B2 (Terrier et al. 2010). The white cross shows the position of the X-ray source IGR J17475-2822. **(Right panel)** 0.1-10 keV image observed with the XMM Newton in April 2007 toward Sgr A (image taken from <http://xmm.esac.esa.int/xsa/index.shtml>). The line shows the position of Sgr A*. AX J1745.6-2901 is the brightest source in the field. The circles with the beam size of the Mopra telescope ($38''$ at 90 GHz) show $LOS+0.693$ and $LOS-0.11$ in the left and right panels, respectively.

of 25. The intermediate CS/HOC⁺ ratio of 6 found in NGC 1068, which is considered to be dominated by X-ray chemistry, is much smaller than the ratio found in $LOS+0.693$ which also shows X-rays, suggesting that the CS/HOC⁺ ratio could be also a good tracer of strong XDR components since the X-ray luminosity in NGC 1068 (Iwasawa et al.

1997) is nearly four orders of magnitude higher than in Sgr B2 (Koyama et al. 1996).

Table 6. Physical parameters derived from H α recombination lines.

Recombination line	ν	Continuum Flux	<i>LOS</i> +0.693		Continuum Flux	<i>LOS</i> −0.11	
			Electron Density	Flux of Lyman Continuum Photons (N_{Lyc})		Electron Density	Flux of Lyman Continuum Photons (N_{Lyc})
	(GHz)	(Jy)	(cm^{-3})	Log(N_{Lyc}) (s^{-1})	(Jy)	(cm^{-3})	Log(N_{Lyc}) (s^{-1})
H43 α	79.912	$\lesssim 1.2$	$\lesssim 473.2$	$\lesssim 48.6$
H42 α	85.688	$\lesssim 1.4$	$\lesssim 513.0$	$\lesssim 48.7$	$\lesssim 2.6$	$\lesssim 715.9$	$\lesssim 49.0$
H41 α	92.034	$\lesssim 1.5$	$\lesssim 531.2$	$\lesssim 48.7$	$\lesssim 1.2$	$\lesssim 480.5$	$\lesssim 48.6$
H39 α	106.737	$\lesssim 0.8$	$\lesssim 391.2$	$\lesssim 48.4$	$\lesssim 1.3$	$\lesssim 501.5$	$\lesssim 48.7$

Table 7. Ratios of HCO $^+$, CS, HOC $^+$ and HCO.

Source	Velocity (km s^{-1})	HCO $^+$ /HOC $^+$	HCO $^+$ /HCO	HCO/HOC $^+$	CS/HCO	CS/HOC $^+$
<i>LOS</i> +0.693	~ 68	546 (175) ^a	9 (3) ^a	62.9 (30.1)	6 (1)	378 (43)
<i>LOS</i> −0.11	~ 20	$\gtrsim 1134$ ^b	$\gtrsim 11$ ^b	...	$\gtrsim 18$	$\gtrsim 1960$
NGC 253	~ 180	80 (30) ^c	5.2 (1.8) ^c	15.4 (7.9)	2 (1) ^d	25 (10) ^d
	~ 280	63 (17) ^c	5.4 (1.3) ^c	11.7 (4.2)	1.1 (0.5) ^d	13 (5) ^d
M 82	~ 310	60 (28) ^c	9.6 (2.8) ^c	6.3 (3.4)	1 ^e	1 ^f
NGC 1068	~ 1100	128 (28) ^c	3.2 (1.2) ^c	40.0 (17.4)	0.3 (0.2) ^g	6 (4) ^g
Horsehead	...	75–200 ^h	1.1 ⁱ	68.2–181.8
Orion Bar (PDR peak)	~ 9.5	< 166 ^j	2.4 ^k	< 69.2	3 ^l	100 ^m
Molecular peak	~ 10.4	400 ^j	4286 ^m
NGC 7023 (PDR peak)	~ 2.7	50–120 ^j	31 ^k	1.6–3.9	2 ⁿ	66 ^o
Molecular peak	...	> 200 ^j	$\gtrsim 61$ ^o
NGC 2023	~ 10.0	1913 ^p	12 ^k	159.4
Diffuse clouds	...	70–120 ^q

^a We have derived the $N_{\text{HCO}^+} = 5.7 (1.3) \times 10^{14} \text{ cm}^{-2}$ from the $N_{\text{HC}^{18}\text{O}^+}$ assuming the $^{16}\text{O}/^{18}\text{O} = 250$ ratio (W&R94). We also have found the $N_{\text{HOC}^+} = 1.1 (0.1) \times 10^{12} \text{ cm}^{-2}$ and $N_{\text{HCO}} = 6.9 (1.4) \times 10^{13} \text{ cm}^{-2}$ in *LOS*+0.693.

^b We have derived the $N_{\text{HCO}^+} = 3.6 (0.8) \times 10^{14} \text{ cm}^{-2}$ from the $N_{\text{HC}^{18}\text{O}^+}$ assuming the $^{16}\text{O}/^{18}\text{O} = 250$ ratio (W&R94). We also have found the $N_{\text{HOC}^+} \lesssim 0.3 \times 10^{12} \text{ cm}^{-2}$ and $N_{\text{HCO}} \lesssim 3.3 \times 10^{13} \text{ cm}^{-2}$ in *LOS*−0.11.

^c Martín et al. (2009b)

^d Estimated from Martín et al. (2006b, 2009b).

^e Estimated from García-Burillo et al. (2002) and Aladro et al. (2011a).

^f Estimated from Fuente et al. (2006) and Aladro et al. (2011a).

^g Estimated from Martín et al. (2009a) and Aladro et al. (2013).

^h Goicoechea et al. (2009).

ⁱ Gerin et al. (2009).

^j Fuente et al. (2003).

^k Schilke et al. (2001).

^l Estimated from Jansen et al. (1995) and Schilke et al. (2001).

^m Estimated from Jansen et al. (1995) and Fuente et al. (2003).

ⁿ Estimated from Fuente et al. (1993) and Schilke et al. (2001).

^o Estimated from Fuente et al. (1993, 2003).

^p Savage & Ziurys (2004).

^q Liszt et al. (2004).

4.2.5 The HCO $^+$ /HOC $^+$ and HCO $^+$ /HCO ratios

The abundance ratios HCO $^+$ /HOC $^+$ and HCO $^+$ /HCO have also been used to estimate the contribution of the UV radiation to the chemistry of molecular clouds. HCO $^+$ /HOC $^+$ ratios of < 166 and 75–200 are measured in the Orion Bar (Fuente et al. 2003) and the Horsehead (Goicoechea et al. 2009), respectively, considered prototypical galactic PDRs. We found much larger HCO $^+$ /HOC $^+$ ratios of 546 (175) and $\gtrsim 1134$ for *LOS*+0.693 and *LOS*−0.11, respectively. These HCO $^+$ /HOC $^+$ ratios derived in both GC sources are also higher than those measured in extragalactic sources. Like for the CS/HOC $^+$ ratio we find that the HCO $^+$ /HOC $^+$ ratio of the molecular peak in the Orion Bar, as well as that of NGC 2023 are close to the values observed in the GC. We consider NGC 2023 to represent the conditions in a prototypical giant molecular cloud, as Savage & Ziurys (2004) have claimed that the PDR position observed is probably embedded in the molecular cloud, therefore the HCO $^+$ /HOC $^+$ ratio would be biased toward the typical cloud unaffected by UV radiation.

The HCO $^+$ /HCO ratios show the same trend than the HCO $^+$ /HOC $^+$ ratios. The HCO $^+$ /HCO ratios are factors of 4–8 (*LOS*+0.693) and $\gtrsim 5$ –10 (*LOS*−0.11) higher than the HCO $^+$ /HCO ratio of 1–2 in typical Galactic PDRs. However, it is not clear why the HCO $^+$ /HCO ratios show smaller differences between both GC sources and galaxies. In our comparison, the PDRs NGC 7023 and NGC 2023 show the highest HCO $^+$ /HCO ratios, which are biased because both sources were observed toward positions where the HCO $^+$ emission arises from the shielded molecular clouds (Schilke et al. 2001; Savage & Ziurys 2004).

The difference found in the HCO $^+$ /HOC $^+$ and HCO $^+$ /HCO ratios between our sample of typical PDRs and *LOS*+0.693 could be due to X-ray induced chemistry in the giant XDR observed toward Sgr B2 in the Fe K α (6.4 keV) line. It has been claimed that the HOC $^+$ and HCO abundances might increase in regions illuminated by X-rays. Usero et al. (2004) argued that XDR chemistry could provide an explanation for the different abundances of HCO $^+$ and HOC $^+$ measured in the Circumnuclear Disk of the AGN

NGC 1068, which also shows strong Fe K α (6.4 keV) line like in $LOS+0.693$. However they found HCO^+/HOC^+ ratios of ~ 40 -100 and the HCO^+/HCO ratio of 3 in the CN of NGC 1068 which are similar to those found in our sample of typical PDRs. Therefore XDR chemistry seems unlikely to explain the large HCO^+/HOC^+ and HCO^+/HCO ratios observed in the GC LOS .

Meijerink et al. (2007) modeled the chemistry induced by PDRs and XDRs in clouds with different Hydrogen column densities and incident FUV/X-ray radiation fields. By using these models they predicted column density ratios for several molecules, including the HCO^+/HOC^+ and HCO^+/HCO ratios. For the Hydrogen column density of $\sim 2 \times 10^{21} \text{ cm}^{-2}$ and G_0 of 10^3 , the PDR model predicts HCO^+/HOC^+ ratios of ~ 100 , which agree with those derived in NGC 7023 and the Orion Bar (Fuentes et al. 2003). For an X-ray flux of $1.6 \text{ erg cm}^{-2} \text{ s}^{-1}$, and a density of 10^4 cm^{-3} , appropriate to $LOS+0.693$, the XDR models of (Meijerink et al. 2007) predict an HCO^+/HOC^+ ratio of ~ 10 in the cloud interior. The predicted ratio is at least a factor of 55 lower than those inferred in both GC sources (see Table 7), indicating that XDR models cannot reproduce the observed HCO^+/HOC^+ ratios found in both GC sources. This result is consistent with the lack of X-ray emission in $LOS-0.11$ (see Fig. 10). The derived HCO^+/HOC^+ ratio of ~ 63 derived in $LOS+0.693$ cannot be used to distinguish between the XDR or PDR scenario since this ratio is close to those of both the Horsehead, a typical PDR, and the claimed XDR NGC 1068. Finally, the HCO^+/HCO ratio of ~ 1 predicted by Meijerink et al. (2007) for PDRs with G_0 of 10^3 is consistent with those in the Horsehead and the Orion Bar (Gerin et al. 2009; Schilke et al. 2001).

In summary, as discussed throughout this section the large HCO^+/HOC^+ , CS/HOC^+ , HCO^+/HCO ratios suggest that the molecular gas affected by X-ray/UV radiation fields in the two GC LOS s represent a small fraction of the total column density of molecular gas. Assuming that the observed HCO^+/HCO ratio of 1.1 in the Horsehead represents the actual PDR ratio, we estimated that roughly $\sim 12\%$ of the total column density would be affected by the UV radiation in $LOS+0.693$ and $\lesssim 10\%$ in $LOS-0.11$. These results also support the HNC/CS diagnostic diagram proposed by Martín et al. (2008, 2009a) to establish the dominant chemistry and the heating mechanism working in molecular clouds since by using this diagram they found that the chemistry and likely the heating of both GC sources are mainly dominated by shocks.

5 CONCLUSIONS

We have used the Mopra telescope to carry out a 3 mm spectral line survey in the selected frequency ranges of ~ 77 -93 GHz and ~ 105 -113 GHz of two lines of sight, $LOS+0.693$ and $LOS-0.11$, toward the Sgr B2 and Sgr A complexes in the Galactic center. The main conclusions of our study are the following:

- We have detected 38 molecular species and 25 isotopologues in $LOS+0.693$ and 34 molecular species and 18 isotopologues in $LOS-0.11$. We have detected for the first time the PDR/XDR tracers HCO and HOC^+ in the quiescent gas in $LOS+0.693$. These two species and the complex organic

molecules HC_2NC and $HCOCH_2OH$ have not been detected toward $LOS-0.11$.

- The molecular excitation, T_{rot} , and the molecular column densities are derived for all detected molecules by using a LTE approximation. The derived T_{rot} varies between ~ 5 and 73 K for both GC sources, but most molecules show $T_{rot} < 20$ K, indicating subthermal excitation. The symmetric rotors, CH_3CN , $^{13}CH_3CN$ and CH_3CCH show the highest T_{rot} of ~ 55 -73 K, consistent with a T_{kin} of ~ 100 K previously derived for the GC clouds.

- Although $LOS+0.693$ and $LOS-0.11$ are separated by more than ~ 120 pc within the GC, $\sim 80\%$ of molecular species detected in both GC sources reveal similar abundances within a factor of 2 and similar excitation conditions.

- We have used the large number of detected isotopologues to derive isotopic ratios of $^{12}C/^{13}C$, $^{14}N/^{15}N$, $^{16}O/^{18}O$, $^{18}O/^{17}O$, $^{29}Si/^{30}Si$ and $^{32}S/^{34}S$ for both GC sources. The derived $^{12}C/^{13}C$, $^{18}O/^{17}O$ and $^{29}Si/^{30}Si$ ratios averaged over both GC sources agree within uncertainties with the “canonical” values for the GC. Our results suggest that isotopic fractionation and/or selective photodissociation do not play any role in the determination of isotopic ratios from molecular column densities.

- The comparison of the excitation conditions derived for both LOS s in the center of our Galaxy and those found in the starburst galaxies NGC 253 and M 82 shows that the molecular gas in the nuclei of these galaxies have similar physical conditions.

- CH_3OH is the molecule which shows the highest abundance difference between both GC LOS s and starburst galaxies by factors of $\sim (1-6) \times 10^2$. The large difference is likely due to its photodissociation by UV radiation in starbursts.

- We have studied the HCO^+/HOC^+ , HCO^+/HCO and CS/HOC^+ ratios in both GC LOS s, typical PDR regions, starburst galaxies and the AGN NGC 1068. We find that these abundances ratios cannot be used to distinguish between the effects of the X-ray and UV radiation on the molecular clouds.

- We also propose that the CS/HOC^+ , HCO^+/HCO and HCO^+/HOC^+ ratios could be used as good tracers of PDR/XDR components in the molecular clouds in the nuclei of galaxies. These ratios can be used to estimate the fraction of the molecular gas affected by the UV radiation. For example, the large HCO^+/HCO ratio found in $LOS+0.693$ indicates a PDR component of $\sim 12\%$ of the total column density.

ACKNOWLEDGMENTS

This work has been partially funded by MICINN grants AYA2010-21697-C05-01 and FIS2012-39162-C06-01, and Astro-Madrid (CAM S2009/ESP-1496). We also thank the Spanish Ministerio de Ciencia e Innovación under project ESP2013-47809-C3-1-R. We are very grateful to the anonymous referee for suggestions and comments, which have greatly improved the paper. S.M. acknowledges the co-funding of this work under the Marie Curie Actions of the European Commission (FP7-COFUND).

REFERENCES

- Aladro R., Martín-Pintado J., Martín S., Mauersberger R., Bayet E. 2011a, *A&A*, 525, A89
- Aladro R., Martín S., Martín-Pintado J., Mauersberger R., Henkel C., Ocaña-Flaquer B., Amo-Baladrón M. A. 2011b, *A&A*, 535, A84
- Aladro R. et al., 2013, *A&A*, 549, A39
- Amo-Baladrón M. A., Martín-Pintado J., Martín S. 2011, *A&A*, 526, A54
- Apponi A. J., Pesch T. C., Ziurys L. M. 1999, *ApJ*, 519, L89
- Bally J., Stark A. A., Wilson R. W. 1987, *ApJS*, 65, 13
- Batrla W., Menten K. M. 1988, *ApJ*, 329, L117
- Belloche A., Müller H. S. P., Menten K. M., Schilke P., Comito C. 2013, *A&A*, 559, A47
- Carral P., Hollenbach D. J., Lord S. D., Colgan S. W. J., Haas M. R., Rubin R. H., Erickson E. F. 1994, *ApJ*, 423, 223
- Churchwell E., Walmsley C. M., Wood D. O. S. 1992, *A&A*, 253, 541
- Coil A. L., Ho P. T. P. 2000, *ApJ*, 533, 245
- De Pree C. G., Gaume R. A., Goss W. M., Claussen M. J. 1996, *ApJ*, 464, 788
- De Pree C. G., Goss W. M., Gaume R. A. 1998, *ApJ*, 500, 847
- Ferrière K., Gillard W., Jean P. 2007, *A&A*, 467, 611
- Ferrière K. 2012, *A&A*, 540, A50
- Fuente A., Martín-Pintado J., Cernicharo J., Bachiller R. 1993, *A&A*, 276, 473
- Fuente A., Rodríguez-Franco A., García-Burillo S., Martín-Pintado J., Black J. H. 2003, *A&A*, 406, 899
- Fuente A., García-Burillo S., Gerin M., Rizzo J. R., Usero A., Teyssier D., Roueff E., Le Boulrot J. 2006, *ApJ*, 641, L105
- Frerking M. A., Langer W. D., Wilson R. W. 1982, *ApJ*, 262, 590
- Friedel D. N., Snyder L. E., Turner B. E., Remijan A. 2004, *ApJ*, 600, 234
- García-Burillo S., Martín-Pintado J., Fuente A., Usero A., Neri R. 2002, *ApJ*, 575, L55
- Gerin M., Goicoechea J. R., Pety J., Hily-Blant P. 2009, *A&A*, 494, 977
- Goicoechea J. R., Rodríguez-Fernández N. J., Cernicharo J. 2004, *ApJ*, 600, 214
- Goicoechea J. R., Pety J., Gerin M., Hily-Blant P., Le Boulrot J. 2009, *A&A*, 489, 771
- Gordon M. A., Berkemann U., Mezger P. G., Zylka R., Haslam C. G. T., Kreysa E., Sievers A., Lemke R. 1993, *A&A*, 280, 208
- Goss W. M., Schwarz U. J., van Gorkom J. H., Ekers R. D. 1985, *MNRAS*, 215, 69
- Güsten R., Walmsley C. M., Ungerechts H., Churchwell E. 1985, *A&A*, 142, 381
- Hasegawa T., Sato F., Whiteoak J. B., Miyawaki R. 1994, *ApJ*, 429, L77
- Herrnstein R. M., Ho P. T. P. 2002, *ApJ*, 579, L83
- Hüttemeister S., Wilson T. L., Bania T. M., Martín-Pintado J. 1993, *A&A*, 280, 255
- Israel F. P., Baas F. 2003, 404, 495
- Iwasawa K., Fabian A. C., Matt G. 1997, *MNRAS*, 289, 443
- Jansen D. J., Spaans M., Hogerheijde M. R., van Dishoeck E. F. 1995, *A&A*, 303, 541
- Knight J. S., Freeman C. G., McEwan M. J., Smith S. C., Adams N. G., Smith D. 1986, *MNRAS*, 219, 89
- Koyama K., Maeda Y., Sonobe T., Takeshima T., Tanaka Y., Yamauchi S. 1996, *PASJ*, 48, 249
- Liszt H., Lucas R., Black J. H. 2004, *A&A*, 428, 117
- Lu F. J., Wang Q. D., Lang C. C. 2003, *AJ*, 126, 319
- Martín-Pintado J., de Vicente P., Wilson T. L., Johnston K. J. 1990, *A&A*, 236, 193
- Martín-Pintado J., de Vicente P., Fuente A., Planesas P. 1997, *ApJ*, 482, L45
- Martín-Pintado J., de Vicente P., Rodríguez-Fernández N. J., Fuente A., Planesas P. 2000, *A&A*, 356, L5
- Martín-Pintado J., Rizzo J. R., de Vicente P., Rodríguez-Fernández N. J., Fuente A. 2001, *ApJ*, 548, L65
- Martín S., Martín-Pintado J., Mauersberger R. 2006a, *A&A*, 450, L13
- Martín S., Mauersberger R., Martín-Pintado J., Henkel C., García-Burillo S. 2006b, *ApJS*, 164, 450
- Martín S., Requena-Torres M. A., Martín-Pintado J., Mauersberger R. 2008, *ApJ*, 678, 245
- Martín S., Martín-Pintado J., Mauersberger R. 2009a, *ApJ*, 694, 610
- Martín S., Martín-Pintado J., Viti S. 2009b, *ApJ*, 706, 1323
- Martín S., Aladro R., Martín-Pintado J., Mauersberger R. 2010, *A&A*, 522, A62
- Mehring D. M., Palmer P., Goss W. M. 1995, *ApJS*, 97, 497
- Meier D. S., Turner J. L. 2005, *ApJ*, 618, 259
- Meier D. S., Turner J. L. 2012, *ApJ*, 755, 104
- Meijerink R., Spaans M., Israel F. P. 2007, *A&A*, 461, 793
- Mezger P. G., Henderson A. P. 1967, *ApJ*, 147, 471
- Mills E., Morris M. R., Lang C. C., Dong H., Wang Q. D., Cotera A., Stolovy S. R. 2011, *ApJ*, 735, 84
- Morris M., Serabyn E. 1996, *ARA&A*, 34, 645
- Mul P. M., McGowan J. W. 1980, *ApJ*, 237, 749
- Müller H. S. P., Thorwirth S., Roth D. A., Winnewisser G. 2001, *A&A*, 370, L49
- Müller H. S. P., Schlöder F., Stutzki J., Winnewisser G. 2005, *J. Molecular Spectroscopy and Structure*, 742, 215
- Nummelin A., Bergman P., Hjalmarsen Å., Friberg P., Irvine W. M., Millar T. J., Ohishi M., Saito S. 1998, *ApJS*, 117, 427
- Nummelin A., Bergman P., Hjalmarsen Å., Friberg P., Irvine W. M., Millar T. J., Ohishi M., Saito S. 2000, *ApJS*, 128, 213
- Pickett H. M., Poynter R. L., Cohen E. A., Delitsky M. L., Pearson J. C., Müller H. S. P. 1998, *J. of Quantitative Spectroscopy and Radiative Transfer*, 60, 883
- Ponti G., Terrier R., Goldwurm A., Belanger G., Trap G. 2010, *ApJ*, 714, 732
- Requena-Torres M. A., Martín-Pintado J., Rodríguez-Franco A., Martín S., Rodríguez-Fernández N. J., de Vicente P. 2006, *A&A*, 455, 971
- Requena-Torres M. A., Martín-Pintado J., Martín S., Morris M. R. 2008, *ApJ*, 672, 352
- Rodríguez-Fernández N. J., Martín-Pintado J., Fuente A., de Vicente P., Wilson T. L., Hüttemeister S. 2001, *A&A*, 365, 174
- Rodríguez-Fernández N. J., Martín-Pintado J., Fuente A., Wilson T. L. 2004, *A&A*, 427, 217

- Riquelme D., Amo-Baladrón M. A., Martín-Pintado J., Mauersberger R., Martín S., Bronfman L. 2010, *A&A*, 523, A51
- Savage C., Ziurys L. M. 2004, *ApJ*, 616, 966
- Schilke P., Pineau des Forêts G., Walmsley C. M., Martín-Pintado J. 2001, *A&A*, 372, 291
- Spaans M., Meijerink R. 2007, *ApJ*, 664, L23
- Sutton E. C., Jaminet P. A., Danchi W. C., Blake G. A. 1991, *ApJS*, 77, 255
- Terrier R., Ponti G., Bélanger G., et al., 2010, *ApJ*, 719, 143
- Turner B. E. 1991, *ApJS*, 76, 617
- Usero A., García-Burillo S., Fuente A., Martín-Pintado J., Rodríguez-Fernández N. J. 2004, *A&A*, 419, 897
- van der Tak F. F. S., Black J. H., Schöier F. L., Jansen D. J., van Dishoeck E. F. 2007, *A&A*, 468, 627
- Wilson T. L., Matteucci F. 1992, *A&ARv*, 4, 1
- Wilson T. L., Rood R. T. 1994, *ARA&A*, 32, 191
- Yusef-Zadeh F., Morris M. 1987, *ApJ*, 320, 545
- Yusef-Zadeh F., Hewitt J. W., Cotton W. 2004, *ApJS*, 155, 421
- Yusef-Zadeh F., Wardle M., Muno M., Law C., Pound M. 2005, *Advances in Space Research*, 35, 1074
- Zuckerman B., Turner B. E., Johnson D. R., Palmer P., Morris M. 1972, *ApJ*, 177, 601